Quaternary Research (2017), 1–17.

doi:10.1017/qua.2017.11

Cosmogenic nuclide age estimate for Laurentide Ice Sheet recession from the terminal moraine, New Jersey, USA, and constraints on latest Pleistocene ice sheet history

Lee B. Corbett[a]*, Paul R. Bierman[a], Byron D. Stone[b], Marc W. Caffee[c,d,e], Patrick L. Larsen[a]

[a]Department of Geology and School of Natural Resources, University of Vermont, Burlington, Vermont 05405, USA
[b]U.S. Geological Survey, East Hartford, Connecticut 06103, USA
[c]Center for Accelerator Mass Spectrometry, Lawrence Livermore National Laboratory, Livermore, California 94550, USA
[d]Department of Physics and Astronomy, Purdue University, West Lafayette, Indiana 47907, USA
[e]Department of Earth, Atmospheric, and Planetary Sciences, Purdue University, West Lafayette, Indiana 47907, USA

(Received July 8, 2016; Accepted January 21, 2017)

Abstract

The time at which the Laurentide Ice Sheet reached its maximum extent and subsequently retreated from its terminal moraine in New Jersey has been constrained by bracketing radiocarbon ages on preglacial and postglacial sediments. Here, we present measurements of in situ produced ^{10}Be and ^{26}Al in 16 quartz-bearing samples collected from bedrock outcrops and glacial erratics just north of the terminal moraine in north-central New Jersey; as such, our ages represent a minimum limit on the timing of ice recession from the moraine. The data set includes field and laboratory replicates, as well as replication of the entire data set five years after initial measurement. We find that recession of the Laurentide Ice Sheet from the terminal moraine in New Jersey began before 25.2 ± 2.1 ka (^{10}Be, n = 16, average, 1 standard deviation). This cosmogenic nuclide exposure age is consistent with existing limiting radiocarbon ages in the study area and cosmogenic nuclide exposure ages from the terminal moraine on Martha's Vineyard ~300 km to the northeast. The age we propose for Laurentide Ice Sheet retreat from the New Jersey terminal position is broadly consistent with regional and global climate records of the last glacial maximum termination and records of fluvial incision.

Keywords: Geochronology; Deglaciation; Ice sheet; Pleistocene; Terminal moraine; Last glacial maximum

INTRODUCTION

The Laurentide Ice Sheet, which covered much of northern North America during the latest Pleistocene glaciation, is thought to have contained about 80 m of global sea-level equivalent at its maximum volume (Clark and Mix, 2002). Understanding the history of the Laurentide Ice Sheet, particularly the timing of the last glacial maximum extent (Clark et al., 2009) and subsequent retreat, is an important step toward clarifying the relationship between global ice volume and sea level. Gaining a better understanding of the relationship between melting ice and rising seas is particularly relevant as we face the prospect of future sea-level rise in response to ice loss in polar regions (Long, 2009; Lambeck et al., 2014).

*Corresponding author at: Department of Geology and School of Natural Resources, University of Vermont, Burlington, Vermont 05405, USA. E-mail address: Ashley.Corbett@uvm.edu (L.B. Corbett).

The time at which the Laurentide Ice Sheet reached its maximum extent and subsequently retreated remains uncertain. Most ages related to last glacial maximum ice extent come from nonglacial sediments either below or above late Wisconsinan till and therefore provide at best a bracketing chronology (Fullerton, 1986; Stone and Borns, 1986; Stone et al., 2005). The North American varve chronology (Ridge et al., 2012) further constrains Laurentide Ice Sheet history; ice margin positions are inferred indirectly using sedimentation patterns in glacial lakes. Several studies use cosmogenic nuclides to date directly the last glacial maximum and initial ice recession in northeastern North America (Balco et al., 2002; Balco and Schaefer, 2006), but reconciling cosmogenic nuclide exposure age chronologies with radiocarbon chronologies is challenging (Peteet et al., 2012). Thus, a conclusive age of the last glacial maximum extent of the Laurentide Ice Sheet in much of northeastern North America remains elusive.

Here, we constrain the age of the Laurentide Ice Sheet maximum extent in north-central New Jersey (Fig. 1),

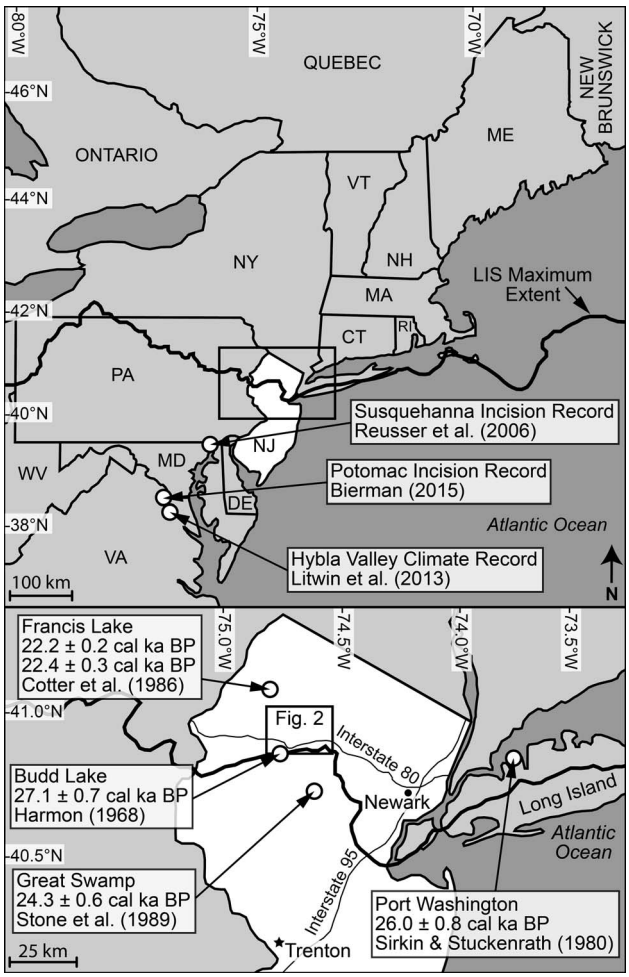

Figure 1. Generalized regional map of the study area, with heavy black line showing the approximate maximum extent of the Laurentide Ice Sheet during the last glacial maximum. Top panel shows the northeastern United States and neighboring Canadian provinces, with climatic and geomorphic records mentioned in the text. Bottom panel shows the northern half of New Jersey with radiocarbon chronology shown in Table 1; black box denotes the extent of Figure 2. Cosmogenic nuclide exposure ages from other studies in northeastern North America are shown in Figure 5.

which was glaciated by the western margin of the Hudson-Champlain lobe (Connally and Sirkin, 1973). We use analysis of cosmogenic nuclides in glacially abraded bedrock surfaces and boulders directly north of (in most cases only a few kilometers from) the terminal moraine; these ages represent a minimum age limit for the timing of ice recession from the moraine. The goal of this work is to constrain the time when the Laurentide Ice Sheet receded from its maximum extent, adding to the existing chronological data from the region, including cosmogenic nuclide exposure ages on the terminal moraine in Martha's Vineyard (~300 km to the northeast) from Balco et al. (2002). We compare cosmogenic nuclide exposure age chronologies and radiocarbon chronologies and explore the regional context of Laurentide Ice Sheet history.

BACKGROUND: CONSTRAINING GLACIAL HISTORY WITH COSMOGENIC NUCLIDES

Cosmogenic nuclides produced in situ, including ^{10}Be and ^{26}Al, have been used extensively to determine the timing of deglaciation (Nishiizumi et al., 1989; Phillips et al., 1990; Bierman, 1994; Gosse et al., 1995a; Fabel and Harbor, 1999; Balco, 2011; Heyman et al., 2011, 2016). These nuclides accumulate at well-constrained rates in rock surfaces exposed to cosmic rays (Lal, 1988); determining the concentration of the nuclide of interest (in this case ^{10}Be and ^{26}Al) in quartz isolated from samples of glacially abraded bedrock or boulder surfaces quantifies the duration of time that has elapsed since deglaciation (Nishiizumi et al., 1993; Gosse and Phillips, 2001). Interpreting a cosmogenic nuclide measurement as an exposure age relies on the assumption that most preexisting nuclides from previous periods of exposure were removed by deep erosion (at least several meters) during the last glaciation and that no postglacial erosion or shielding of the surface has occurred. Violations of these assumptions cause overestimates or underestimates of actual exposure ages and thus increase the variance of calculated nuclide concentrations and exposure ages, limiting the precision and accuracy of moraine age estimates.

Cosmogenic nuclides have proved useful in constraining the chronology of Laurentide Ice Sheet glaciation and deglaciation in North America, as reviewed by Briner et al. (2006a). The use of ^{10}Be (and sometimes ^{26}Al) has helped to determine the age of moraines and other glacial/postglacial features in Maine (Bierman et al., 2015; Bromley et al., 2015; Davis et al., 2015; Koester et al., 2017), New Hampshire (Bierman et al., 2015; Bromley et al., 2015), Massachusetts (Balco et al., 2002), Connecticut (Balco and Schaefer, 2006), Wisconsin (Ullman et al., 2015), Baffin Island (Steig et al., 1998; Davis et al., 1999; Marsella et al., 2000; Kaplan et al., 2001; Kaplan and Miller, 2003), and northeastern mainland Canada (Clark et al., 2003). ^{10}Be has been used to study Laurentide Ice Sheet ice margin retreat rates, including episodes of rapid ice loss in Baffin Island (Briner et al., 2009) and Labrador (Carlson et al., 2007; Ullman et al., 2016). Paired ^{26}Al/^{10}Be analysis of stacked buried tills in the midwestern United States has clarified glaciation timing and extent over several million years (Balco et al., 2005a, 2005b; Balco and Rovey, 2008, 2010).

In regions where the Laurentide Ice Sheet was cold based and nonerosive, the use of multiple cosmogenic nuclides (^{10}Be, ^{26}Al, and/or ^{14}C) provides insight about subglacial erosion efficacy and the long-term preservation of glacially buried surfaces. Multinuclide approaches have been especially useful in Baffin Island, where much of the Laurentide Ice Sheet seems to have been cold based (Bierman et al., 1999; Briner et al., 2003, 2005, 2006b, 2014; Miller et al., 2006; Corbett et al., 2016a; Margreth et al., 2016). In addition to Baffin Island, the existence of a cold-based Laurentide Ice Sheet has been documented using a multiple nuclide approach in mainland Canada (Gosse et al., 1993, 1995b; Marquette et al., 2004; Staiger et al., 2005) and near the

margin in the midwestern United States (Bierman et al., 1999; Colgan et al., 2002). In the northeastern United States, cold-based ice exited only on the highest summits (Bierman et al., 2015), where ice was likely thin and flow was not channelized.

STUDY AREA

Our work focuses on three sample sites (Fig. 2) in the Highlands of north-central New Jersey: Picatinny Arsenal, Allamuchy State Forest, and Weldon Road. Two erosion-resistant rock types, Precambrian gneiss and Paleozoic quartzite, dominate the area (Drake et al., 1996). At Picatinny Arsenal, the Silurian Green Pond Conglomerate (characterized by quartz pebbles and cobbles in a quartz sand matrix) forms sharp-crested, northeast-trending ridges. The Precambrian Losee Metamorphic Suite, which underlies the Allamuchy State Forest and Weldon Road sites, is characterized by light color and granitic composition. Surficial materials in upland areas include thin, sandy till and scattered slope deposits (Stanford and Witte, 2006).

Glacial erosion in the New Jersey Highlands has produced an upland landscape characterized by numerous large, fresh, polished bedrock outcrops discontinuously covered by thin, patchy till. Upland striations in the study area range in azimuth from 178° to 194° (Fig. 2); these striations record glacial flow normal to the local trend of the terminal moraine a few kilometers to the south. Results of detailed geologic mapping (Stanford, 1993; Stone et al., 1995) confirm the extent, thickness, and distinct surface morphological features of the terminal moraine originally described by Salisbury (1902) in the area of our sample sites.

Deposits of the Budd Lake segment of the terminal moraine (Stone et al., 2002) extend in a belt 0.8–3.5 km wide across the area (Fig. 2; see also Supplementary Figure 1). The moraine segment rises from 195 meters above sea level (m asl) in the valley on the east side of the study area to a maximum of 367 m asl and reaches to 360 m asl on the west side of the area. The moraine averages ~24 m in height above adjacent ground but has a maximum height of ~68 m in valleys. It is composed mostly of till but also contains stratified sediments, flow till, and colluvial deposits; transverse ridges and ridge-and-kettle features may be related to ice margin sediment transport, deposition, and deformation processes during moraine construction (Stone et al., 2002).

PREVIOUS WORK: GLACIAL CHRONOLOGY IN THE NORTHEASTERN UNITED STATES

Radiocarbon chronology

The timing of glacial advance has been constrained throughout the northeastern United States with radiocarbon dating. The advancing margin of the Laurentide Ice Sheet likely first entered the northeastern United States through the Champlain Valley ~30–29 ^{14}C ka BP (~35–34 cal ka BP) (Parent et al., 2015; Rayburn et al., 2015) and entered Maine ~29–24 ^{14}C ka BP (~33–28 cal ka BP) (Anderson et al., 1986, 1992; Dorion, 1997), as reviewed and recalibrated in

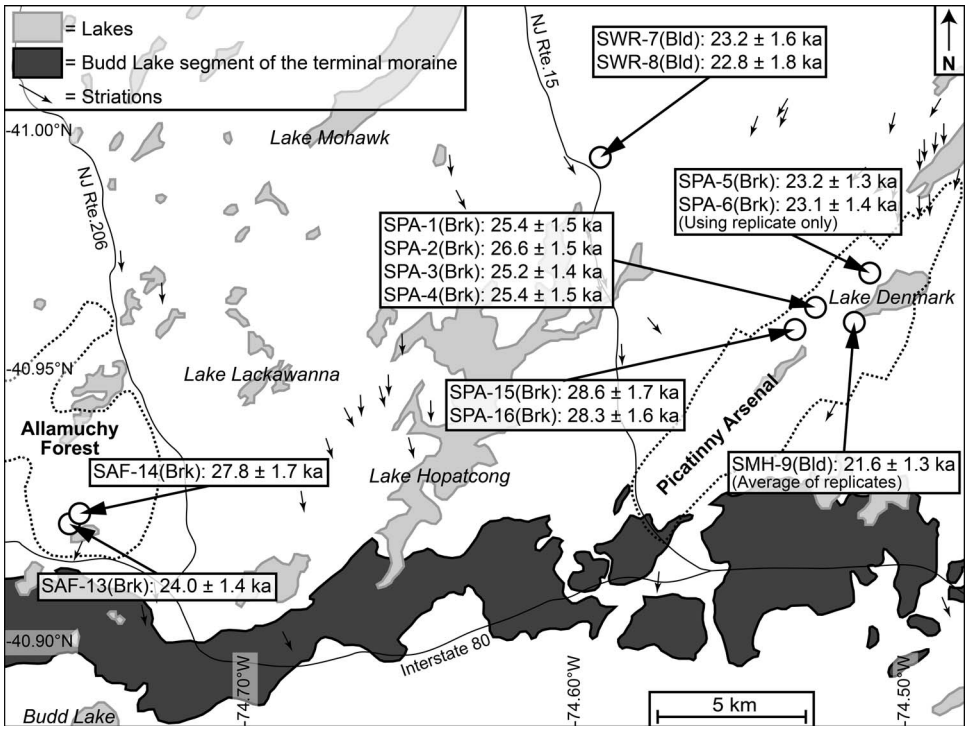

Figure 2. Map of the study area, including the Budd Lake segment of the terminal moraine and striation directions from Stone et al. (2002). Sample sites show ^{10}Be ages and 1σ external uncertainties; "Brk" and "Bld" denote bedrock and boulder samples, respectively. A detailed map of the study area is shown in Supplementary Figure 1.

Bierman et al. (2015). The Hudson-Champlain lobe of the Laurentide Ice Sheet advanced into the northern New Jersey region ~23–22 ^{14}C ka BP (~28–26 cal ka BP) (Fullerton, 1986; Stone and Borns, 1986; Stone et al., 2002; Rayburn et al., 2015). The glacial margin then spread westward into the New Jersey Highlands from its axis in the Hudson River lowland. Striations on upland surfaces in the New Jersey Highlands (Stanford, 1993) and across the study area (Stone et al., 2002) show that the ice flowed southward across northern New Jersey, reaching its terminal position ~22–21 ^{14}C ka BP (26–25 cal ka BP) (Connally and Sirkin, 1973; Stone et al., 1989, 1995, 2002; Stanford, 1993).

In addition to constraining the timing of Laurentide Ice Sheet advance, regional radiocarbon chronologies have also illustrated the timing and pattern of ice margin retreat. The radiocarbon-dated North American varve chronology, developed throughout western New England (Ridge et al., 2012), has been particularly useful for dating the recession of the Laurentide Ice Sheet margin. In southern New York, the oldest correlated varve provides a minimum limit of ~18.8 ka for the timing of ice retreat for our study site to the southwest. The remaining chronology, biased toward the Connecticut River Valley (and hence not along the same flow line as our study site) shows the ice margin entering southern Massachusetts ~17.7 ka, crossing into Vermont and New Hampshire ~15.5 ka, and ultimately reaching the Canadian border ~13.4 ka (see fig. 12 in Ridge et al. 2012).

In or near the study area, radiocarbon ages of organic material in preglacial and postglacial sediments constrain the age of the terminal moraine in the New Jersey Highlands, as summarized and recalibrated in Table 1 and Figure 1. Pollen-bearing bulk preglacial sediments from northern Long Island (Sirkin and Stuckenrath, 1980) provide a maximum limiting radiocarbon age of 21.75 ± 0.75 ^{14}C ka BP (26.02 ± 0.81 cal ka BP).

Minimum limiting age constraints come from south of, within, and north of the terminal moraine. Outside the glacial limit, a concretion in varved sediments of glacially dammed Lake Passaic (Great Swamp) yielded a radiocarbon age of 20.18 ± 0.50 ^{14}C ka BP (24.31 ± 0.63 cal ka BP) (Stone et al., 1989). Concretions can contain old, reworked carbon with the potential to bias ages; although the dates in this core are in stratigraphic order, with a stratigraphically higher concretion yielding a radiocarbon age of 14.06 ± 0.24 ^{14}C ka BP (17.09 ± 0.36 cal ka BP) (Stone et al., 2002), it is possible that they do not reflect accurately the age of the lake.

Basal lake clay with gyttja from Budd Lake, also impounded along the terminal moraine, yielded a radiocarbon age of 22.89 ± 0.72 ^{14}C ka BP (27.07 ± 0.67 cal ka BP) (Harmon, 1968). Again, although this bulk sediment date may contain older carbon not directly related to the age of the lake, ages here are also in stratigraphic order; a younger organic layer in pollen-bearing beds returned an age of 12.29 ± 0.50 ^{14}C ka BP (14.44 ± 0.72 cal ka BP) (Stone et al., 2002).

Inside the glacial limit, basal bulk sediments from Francis Lake yielded radiocarbon ages of 18.39 ± 0.20 and

Table 1. Compilation of recalibrated radiocarbon ages constraining the timing of Laurentide Ice Sheet maximum extent and subsequent recession in the study area.

Location	Latitude (°N)	Longitude (°E)	Dated material	Age (1σ, ^{14}C yr BP)	Calibrated age (1σ range, cal yr BP)[a]	Calibrated age (midpoint ± half of 1σ range, cal yr BP)[a]	Reference	Age type[b]
Long Island	40.82	−73.70	Organic silt	21,750 ± 750	25,300–26,920	26,020 ± 810	Sirkin and Stuckenrath (1980)	Stratigraphic maximum
Budd Lake	40.87	−74.75	Bulk sediment	22,890 ± 720	26,390–27,720	27,070 ± 670	Harmon (1968)	Stratigraphic minimum
Budd Lake	40.87	−74.75	Bulk sediment	12,290 ± 500	13,720–15,160	14,440 ± 720	Stone et al. (2002)	Postglacial
Francis Lake	40.98	−74.84	Bulk sediment	18,390 ± 200	22,010–22,440	22,230 ± 220	Cotter et al. (1986)	Stratigraphic minimum
Francis Lake	40.98	−74.84	Bulk sediment	18,570 ± 250	22,150–22,740	22,430 ± 300	Cotter et al. (1986)	Stratigraphic minimum
Francis Lake	40.98	−74.84	Bulk sediment	16,480 ± 430	19,380–20,430	19,910 ± 530	Stone et al. (2002)	Postglacial
Francis Lake	40.98	−74.84	Bulk sediment	13,510 ± 140	16,060–16,480	16,270 ± 210	Stone et al. (2002)	Postglacial
Francis Lake	40.98	−74.84	Bulk sediment	11,220 ± 110	12,980–13,220	13,100 ± 120	Stone et al. (2002)	Postglacial
Great Swamp	40.87	−74.75	Concretion	20,180 ± 500	23,710–24,970	24,310 ± 630	Stone et al. (1989)	Stratigraphic minimum
Great Swamp	40.87	−74.75	Concretion	14,060 ± 240	16,730–17,440	17,090 ± 360	Stone et al. (2002)	Postglacial

[a]Ages have been calibrated using the online Calib program version 7.1 and the IntCal13 calibration curve (Reimer et al., 2013).
[b]Refers to whether the radiocarbon age represents a maximum or minimum limit for the age of the Laurentide Ice Sheet terminal moraine in the study area. See text for details.

18.57 ± 0.25 ^{14}C ka BP (22.23 ± 0.22 and 22.43 ± 0.30 cal ka BP) (Evenson et al., 1983; Cotter et al., 1986). Overlying clay beds yielded upward-younging ages of 16.48 ± 0.43 ^{14}C ka BP (19.91 ± 0.53 cal ka BP) and 13.51 ± 0.14 ^{14}C ka BP (16.27 ± 0.21 cal ka BP) and were capped by peaty gyttja dating to 11.22 ± 0.11 ^{14}C ka BP (13.10 ± 0.12 cal ka BP).

Using radiocarbon ages to infer Laurentide Ice Sheet advance and retreat has limitations (Peteet et al., 2012). First, the unknown lag time between ice margin retreat and the onset of organic matter deposition may make minimum age limits too young (Davis and Davis, 1980). The scarcity of organic material in postglacial sediments because of cold conditions also limits the utility of basal radiocarbon ages for developing accurate deglaciation chronologies (Cotter et al., 1986; Stone and Borns, 1986; Balco and Schaefer, 2006). Additionally, carbon unrelated to the material being dated can contaminate the sample, especially in the case of bulk sediments or concretions (Grimm et al., 2009). If the existing radiocarbon age control is correct, one would expect cosmogenic nuclide exposure ages between ~26.0 ka (Sirkin and Stuckenrath, 1980) and ~22.2 ka (Cotter et al., 1986). However, it is important to note that our exposure ages also represent a minimum limit because the sampled surfaces are slightly north of the terminal moraine (Fig. 2).

Regional cosmogenic nuclide exposure age chronology

In addition to radiocarbon dating of organic material, cosmogenic nuclides produced in situ have been employed to determine the timing of maximum ice extent and subsequent ice margin retreat in northeastern North America. In coastal Massachusetts, Balco et al. (2002) used the exposure ages of boulders along the Martha's Vineyard terminal moraine to estimate an age of 27.5 ± 2.2 ka (^{10}Be, n = 8, average, 1 standard deviation [SD]; ages have been recalculated using the northeastern North American production rates of Balco et al. [2009]). Southern New England recessional moraines have been dated with cosmogenic ^{10}Be, including the Buzzard's Bay moraine in Massachusetts (20.3 ± 1.2 ka, n = 10; Balco et al., 2002) and the Ledyard (20.7 ± 0.7 ka, n = 7; Balco and Schaefer, 2006) and Old Saybrook (20.7 ± 0.9 ka, n = 7; Balco and Schaefer, 2006) moraines in Connecticut (all ages are average ± 1 SD and have been recalculated using the northeastern North American production rates). Dates in Maine show that the Basin Ponds moraine near Katahdin was abandoned 16.1 ± 1.2 ka (^{10}Be, n = 5, average, 1 SD), and the summit of Katahdin became exposed 15.3 ± 2.1 ka (^{10}Be, n = 6, average, 1 SD), suggesting that ice thinning exposed these high areas relatively early (Davis et al., 2015). The Laurentide Ice Sheet margin reached coastal Maine around the same time, exposing Acadia National Park 15.2 ± 0.7 ka (^{10}Be, n = 16, average, 1 SD) and forming the Pineo Ridge moraine 14.5 ± 0.7 ka (^{10}Be, n = 7, average, 1 SD; Koester et al. 2017). The retreating ice sheet then exposed the Littleton-Bethlehem moraine in central-northern New Hampshire at 13.8 ± 0.2 ka (^{10}Be, n = 4, average, 1 SD) and the Androscoggin moraine in northeastern New Hampshire and western Maine at 13.2 ± 0.4 ka (^{10}Be, n = 7, average, 1 SD), as described in Bromley et al. (2015).

Like radiocarbon ages, cosmogenic nuclide exposure ages have limitations. Geologic variance because of processes such as moraine crest degradation and boulder surface erosion can lead to a spread of ages rather than a clearly defined central tendency (Applegate et al., 2010, 2012; Heyman et al., 2011). Inherited nuclides from previous periods of exposure, especially but not exclusively in rock surfaces that glacial ice failed to deeply erode, lead to age overestimates (Heyman et al., 2011; Briner et al., 2016). Cover by snow and/or sediment can shield sample surfaces from postglacial nuclide production, causing age underestimates (Schildgen et al., 2005; Heyman et al., 2016). Because of limitations with both radiocarbon and cosmogenic nuclide exposure age chronologies, reconciling findings between the two has been a challenge (Peteet et al., 2012).

METHODS

Study design and field sampling

Samples were collected using a hammer and chisel from three separate areas immediately north of the Budd Lake moraine segment (Stone et al., 2002) in north-central New Jersey during the summer of 1994 (Fig. 2). Nine samples were taken from Picatinny Arsenal, approximately 4 km north of the moraine; eight of these (SPA-1, -2, -3, -4, -5, -6, -15, and -16) were of bedrock from prominent ridges, and one (SMH-9) was from a boulder at lower elevation, near Lake Denmark. Five samples were taken from Allamuchy State Forest <1 km north of the moraine: two of these (SAF-10 and -11) were from the same ridgetop boulder, SAF-12 came from an adjacent boulder, and two additional samples (SAF-13 and -14) were from a nearby bedrock ridge. Two additional samples (SWR-7 and -8) were taken from a large erratic near Weldon Road ~9 km north of the moraine.

To minimize the likelihood of past till cover over bedrock samples, we selected bedrock surfaces that were either dipping or located on a prominent ridgetop or near a cliff edge. To minimize the likelihood of postdepositional movement or till cover of boulder samples, we selected only the largest boulders (~1.5–2 m in height; see Larsen, 1996 for sample photographs, diagrams, and descriptions) that were near or atop ridges. Sample locations and elevations were estimated using 1:24,000-scale topographic maps (Table 2). Field observations included sample thickness and slope of the sampled surface (Table 2).

Sample preparation

Sixteen samples were prepared at the University of Vermont in 1995 (as reported in Larsen, 1996; Clark et al., 1995) and prepared again in 2000. The data from 1995 are presented in Supplementary Table 1. In this manuscript, we focus on the higher-precision analyses from 2000 (Tables 3 and 4).

Table 2. Sample collection information for the 16 samples (plus two replicates) investigated in this study.

Sample name	Site	Lithology	Type	Elevation (m)	Latitude (°N)	Longitude (°E)	Sample thickness (cm)	Surface dip (°)
SAF-10	Allamuchy Forest	Gneiss	Boulder	323	40.92176	–74.74992	2.5	22
SAF-11	Allamuchy Forest	Gneiss	Boulder	323	40.92176	–74.74992	5.0	0
SAF-12	Allamuchy Forest	Gneiss	Boulder	323	40.92176	–74.74992	3.0	0
SAF-13	Allamuchy Forest	Gneiss	Bedrock	299	40.92088	–74.75086	6.0	30
SAF-14	Allamuchy Forest	Gneiss	Bedrock	278	40.92104	–74.74943	3.0	0
SMH-9[a]	Picatinny Arsenal	Quartzite	Boulder	253	40.96378	–74.52785	2.5	15
SPA-1	Picatinny Arsenal	Quartzite	Bedrock	342	40.96619	–74.53888	1.5	0
SPA-2	Picatinny Arsenal	Quartzite	Bedrock	342	40.96619	–74.53888	5.0	0
SPA-3	Picatinny Arsenal	Quartzite	Bedrock	342	40.96619	–74.53888	1.5	0
SPA-4	Picatinny Arsenal	Quartzite	Bedrock	342	40.96619	–74.53888	3.0	0
SPA-5	Picatinny Arsenal	Quartzite	Bedrock	336	40.97425	–74.52339	4.5	20
SPA-6[a]	Picatinny Arsenal	Quartzite	Bedrock	336	40.97425	–74.52339	4.5	0
SPA-15	Picatinny Arsenal	Quartzite	Bedrock	336	40.96227	–74.54465	3.0	0
SPA-16	Picatinny Arsenal	Quartzite	Bedrock	336	40.96227	–74.54465	3.0	29
SWR-7	Weldon Road	Gneiss	Boulder	375	40.99768	–74.60282	3.0	0
SWR-8	Weldon Road	Gneiss	Boulder	375	40.99768	–74.60282	3.0	0

[a]Denotes a sample that has a laboratory duplicate.

We prepared laboratory duplicates for samples SPA-6 and SMH-9, resulting in 18 total paired $^{26}Al/^{10}Be$ analyses.

In 2000, we isolated quartz following standard procedures (Kohl and Nishiizumi, 1992), quantified quartz purity using inductively coupled plasma optical emission spectrometry (ICP-OES), and extracted Be and Al as described in Bierman and Caffee (2002) in three separate batches, with each batch including two fully processed blanks. We dissolved ~20–40 g of quartz after adding ~250 µg ^{9}Be (1000 ppm SPEX Be standard) and ^{27}Al as necessary (1000 ppm SPEX Al standard, added to the two samples with low native Al and to all blanks). Total ^{27}Al was quantified in all samples (Table 3) using ICP-OES analysis of small replicate aliquots removed following dissolution as described in Bierman and Caffee (2002).

Isotopic analysis

Isotopic ratios ($^{10}Be/^{9}Be$ and $^{26}Al/^{27}Al$) were measured by accelerator mass spectrometry (AMS) at Lawrence Livermore National Laboratory in 1995 (Supplementary Table 1; as reported in Larsen 1996) and in 2000 (Tables 3 and 4; as

Table 3. Sample preparation and accelerator mass spectrometry information (second set of analyses, year 2000) for the 16 samples plus two replicates investigated in this study. See Supplementary Table 2 and Supplementary Figure 2 for more detail about blanks. The original analyses (from the year 1995) are provided in Supplementary Table 1.

Sample name	Quartz mass (g)	^{9}Be added (µg)	ICP-quantified total ^{27}Al (µg)	Be cathode number	Al cathode number	Measured $^{10}Be/^{9}Be$[a]	$^{10}Be/^{9}Be$ uncertainty[a]	Measured $^{26}Al/^{27}Al$[a]	$^{26}Al/^{27}Al$ uncertainty[a]
SAF-10	41.728	250	3049	BE12519	AL7714	3.63×10^{-13}	7.00×10^{-15}	5.06×10^{-13}	1.45×10^{-14}
SAF-11	40.016	250	2927	BE12520	AL7715	3.55×10^{-13}	5.84×10^{-15}	4.92×10^{-13}	1.47×10^{-14}
SAF-12	26.085	252	2636	BE12527	AL7722	2.50×10^{-13}	6.87×10^{-15}	4.33×10^{-13}	2.12×10^{-14}
SAF-13	39.620	252	2566	BE12528	AL7723	3.11×10^{-13}	5.21×10^{-15}	5.29×10^{-13}	2.99×10^{-14}
SAF-14	28.230	251	2365	BE12529	AL7724	2.69×10^{-13}	4.78×10^{-15}	4.60×10^{-13}	2.74×10^{-14}
SMH-9	39.249	251	4949	BE12521	AL7716	2.89×10^{-13}	5.40×10^{-15}	2.43×10^{-13}	9.04×10^{-15}
SMH-9-DUP	39.826	252	4500	BE12530	AL7725	2.82×10^{-13}	5.20×10^{-15}	2.80×10^{-13}	1.32×10^{-14}
SPA-1	39.560	252	8794	BE12535	AL7730, AL7759	3.57×10^{-13}	9.38×10^{-15}	1.72×10^{-13}	6.52×10^{-15}
SPA-2	40.120	252	8154	BE12536	AL7731	3.67×10^{-13}	8.37×10^{-15}	1.95×10^{-13}	7.90×10^{-15}
SPA-3	39.290	252	8241	BE12537	AL7732	3.53×10^{-13}	6.48×10^{-15}	1.72×10^{-13}	1.01×10^{-14}
SPA-4	39.630	252	8639	BE12538	AL7733, AL7758	3.54×10^{-13}	7.59×10^{-15}	1.73×10^{-13}	6.11×10^{-15}
SPA-5	39.664	252	6257	BE12539	AL7734	3.19×10^{-13}	5.72×10^{-15}	2.03×10^{-13}	7.35×10^{-15}
SPA-6	39.932	252	7748	BE12522	AL7718, AL7754	3.48×10^{-13}	6.86×10^{-15}	1.34×10^{-13}	5.27×10^{-15}
SPA-6-DUP	39.875	253	10,667	BE12540	AL7735	3.21×10^{-13}	6.79×10^{-15}	1.17×10^{-13}	8.28×10^{-15}
SPA-15	40.020	253	10,409	BE12531	AL7726, AL7757	3.95×10^{-13}	9.53×10^{-15}	1.49×10^{-13}	7.67×10^{-15}
SPA-16	39.480	247	8470	BE12532	AL7727, AL7755	3.88×10^{-13}	8.92×10^{-15}	2.07×10^{-13}	6.64×10^{-15}
SWR-7	22.320	251	2192	BE12523	AL7717	2.01×10^{-13}	5.60×10^{-15}	3.82×10^{-13}	1.78×10^{-14}
SWR-8	22.310	252	2626	BE12524	AL7719	1.98×10^{-13}	4.48×10^{-15}	3.19×10^{-13}	1.49×10^{-14}

Note: ICP, inductively coupled plasma.
[a]Ratios were normalized to standard LLNL1000 for Be and KNSTD9919 for Al and have not been corrected for backgrounds.

Table 4. Isotopic concentrations and age information (second set of analyses, year 2000) for the 16 samples plus two replicates investigated in this study. Note that for the purposes of discussion and figures, ages from sample SMH-9 and its replicate SMH-9-DUP have been averaged, whereas the data from sample SPA-6 have been discarded in favor of the data from its replicate SPA-6-DUP.

Sample name	^{10}Be concentration (atoms/g)[a]	^{10}Be uncertainty (atoms/g)[a]	07KNSTD ^{10}Be concentration (atoms/g)[a,b]	07KNSTD ^{10}Be uncertainty (atoms/g)[a,b]	^{26}Al concentration (atoms/g)[a]	^{26}Al uncertainty (atoms/g)[a]	^{10}Be exposure Age (ka)[c]	^{10}Be internal uncertainty (ka)[c]	^{10}Be external uncertainty (ka)[c]	^{26}Al exposure age (ka)[c]	^{26}Al internal uncertainty (ka)[c]	^{26}Al external uncertainty (ka)[c]	07KNSTD ^{26}Al/^{10}Be[b]	07KNSTD ^{26}Al/^{10}Be uncertainty[b]
SAF-10	1.33×10^{5}	3.88×10^{3}	1.24×10^{5}	3.62×10^{3}	8.12×10^{5}	2.35×10^{4}	25.1	0.7	1.4	24.4	0.7	1.4	6.57	0.27
SAF-11	1.35×10^{5}	3.72×10^{3}	1.26×10^{5}	3.47×10^{3}	7.90×10^{5}	2.37×10^{4}	25.9	0.7	1.4	24.0	0.7	1.4	6.29	0.26
SAF-12	1.42×10^{5}	6.20×10^{3}	1.32×10^{5}	5.77×10^{3}	9.60×10^{5}	4.73×10^{4}	26.8	1.2	1.7	28.8	1.4	2.0	7.27	0.48
SAF-13	1.19×10^{5}	3.62×10^{3}	1.11×10^{5}	3.37×10^{3}	7.53×10^{5}	4.27×10^{4}	24.0	0.7	1.4	24.1	1.4	1.8	6.80	0.44
SAF-14	1.42×10^{5}	4.92×10^{3}	1.32×10^{5}	4.58×10^{3}	8.46×10^{5}	5.06×10^{4}	27.8	1.0	1.7	26.4	1.6	2.0	6.41	0.44
SMH-9	1.10×10^{5}	3.69×10^{3}	1.03×10^{5}	3.44×10^{3}	6.69×10^{5}	2.52×10^{4}	22.1	0.7	1.3	21.2	0.8	1.3	6.52	0.33
SMH-9-DUP	1.06×10^{5}	3.60×10^{3}	9.88×10^{4}	3.35×10^{3}	6.92×10^{5}	3.29×10^{4}	21.2	0.7	1.3	21.9	1.1	1.5	7.00	0.41
SPA-1	1.38×10^{5}	4.89×10^{3}	1.29×10^{5}	4.55×10^{3}	8.31×10^{5}	3.21×10^{4}	25.4	0.9	1.5	24.1	0.9	1.5	6.44	0.34
SPA-2	1.41×10^{5}	4.49×10^{3}	1.31×10^{5}	4.18×10^{3}	8.64×10^{5}	3.55×10^{4}	26.6	0.9	1.5	25.9	1.1	1.7	6.59	0.34
SPA-3	1.37×10^{5}	4.00×10^{3}	1.28×10^{5}	3.73×10^{3}	7.82×10^{5}	4.70×10^{4}	25.2	0.7	1.4	22.7	1.4	1.8	6.11	0.41
SPA-4	1.37×10^{5}	4.30×10^{3}	1.27×10^{5}	4.00×10^{3}	8.18×10^{5}	2.95×10^{4}	25.4	0.8	1.5	24.0	0.9	1.5	6.42	0.31
SPA-5	1.22×10^{5}	3.75×10^{3}	1.14×10^{5}	3.49×10^{3}	6.99×10^{5}	2.57×10^{4}	23.2	0.7	1.3	21.0	0.8	1.3	6.14	0.29
SPA-6	1.33×10^{5}	4.05×10^{3}	1.24×10^{5}	3.77×10^{3}	5.61×10^{5}	2.27×10^{4}	25.2	0.8	1.4	16.7	0.7	1.1	4.51	0.23
SPA-6-DUP	1.23×10^{5}	4.05×10^{3}	1.14×10^{5}	3.77×10^{3}	6.73×10^{5}	4.90×10^{4}	23.1	0.8	1.4	20.1	1.5	1.8	5.89	0.47
SPA-15	1.53×10^{5}	4.91×10^{3}	1.43×10^{5}	4.57×10^{3}	8.41×10^{5}	4.41×10^{4}	28.6	0.9	1.7	24.9	1.3	1.8	5.89	0.36
SPA-16	1.49×10^{5}	4.65×10^{3}	1.39×10^{5}	4.33×10^{3}	9.66×10^{5}	3.15×10^{4}	28.3	0.9	1.6	29.2	1.0	1.7	6.97	0.31
SWR-7	1.29×10^{5}	6.58×10^{3}	1.20×10^{5}	6.13×10^{3}	8.23×10^{5}	3.86×10^{4}	23.2	1.2	1.6	23.5	1.1	1.6	6.87	0.48
SWR-8	1.27×10^{5}	6.12×10^{3}	1.18×10^{5}	5.70×10^{3}	8.21×10^{5}	3.86×10^{4}	22.8	1.1	1.6	23.5	1.1	1.6	6.97	0.47

[a] All presented isotopic concentrations have been corrected for backgrounds as described in the text.
[b] Refers to isotopic concentrations that have been scaled to match the currently accepted standard value (07KNSTD; Nishiizumi et al., 2007).
[c] Simple exposure ages and uncertainties were calculated in the CRONUS Earth calculator (Balco et al., 2008) using northeastern North American production rates (Balco et al., 2009).

described here). In the latter set of data (from the year 2000), Be analyses were normalized to standard LLNL1000, and Al analyses were normalized to standard KNSTD9919. The latter set of $^{10}Be/^{9}Be$ sample ratios (measured in 2000; Table 3) ranged from 2.0×10^{-13} to 4.0×10^{-13}, and 1σ AMS measurement precisions were $2.1 \pm 0.4\%$ (n = 18, average, 1 SD). Measured sample $^{26}Al/^{27}Al$ ratios (Table 3) ranged from 1.2×10^{-13} to 5.3×10^{-13} with 1σ AMS measurement precisions of $4.5 \pm 1.2\%$ (n = 18, average, 1 SD).

To correct for laboratory and machine backgrounds, we used the mean ratio (± 1 SD) of blanks processed in the three batches (see Supplementary Table 2 and Supplementary Fig. 2 for detailed information about blanks). The background values utilized for all samples measured in 2000 were $2.81 \pm 0.69 \times 10^{-14}$ for ^{10}Be (n = 6) and $2.60 \pm 0.54 \times 10^{-15}$ for ^{26}Al (n = 3). Using a batch-by-batch blank correction instead of the mean blank has little impact on the resulting isotopic concentrations. Sensitivity analysis demonstrates that using a batch-by-batch blank correction instead of the average blank value changes inferred ^{10}Be concentrations by $1.7 \pm 1.3\%$ and ^{26}Al concentrations by $0.2 \pm 0.1\%$ (n = 18, average, 1 SD; see Supplementary Table 3). For the two sets of laboratory duplicates (SPA-6 and SPA-6-DUP; SMH-9 and SMH-9-DUP), calculated ^{10}Be concentrations are more similar between duplicates using the mean blank correction rather than the batch-by-batch blank correction (Supplementary Table 3), supporting our decision to use the mean blank ratio for background correction.

The mass of purified Al from five of the samples (SPA-1, SPA-4, SPA-6, SPA-15, and SPA-16) was large enough to allow preparation of two separate cathodes (Table 3). These duplicate cathodes were run and normalized as described previously, and the resulting analytical runs were combined as if all data had been collected from a single cathode. The increased number of ^{26}Al counts, over what could have been obtained from a single cathode, reduced the uncertainty in the final measured $^{26}Al/^{27}Al$ ratio.

Because of changes in the nominal $^{10}Be/^{9}Be$ ratio of standards used to normalize isotopic measurements through the years (Nishiizumi et al., 2007), these samples (analyzed in 2000) were normalized to different standard values than are accepted today. To make these data comparable to modern data sets, we scaled all ^{10}Be data to the newer standard value (07KNSTD; Nishiizumi et al., 2007). In the text, we focus on ^{10}Be concentrations and $^{26}Al/^{10}Be$ ratios scaled to the currently accepted values for standards; however, both the measured and rescaled data are presented in Table 4.

Exposure age calculations

We calculated ^{10}Be and ^{26}Al exposure ages (Table 4) using the CRONUS Earth online exposure age calculator (Balco et al., 2008), version 2.2 and constants version 2.2.1, based on analyses from 2000 only. We used the regionally calibrated northeastern North American sea-level production rates of 3.93 ± 0.19 atoms/g/yr for ^{10}Be and 26.5 ± 1.3 atoms/g/yr for ^{26}Al (Balco et al., 2009) and the Lal/Stone constant production rate model and scaling scheme (Lal, 1991; Stone, 2000). We made corrections for latitude, elevation, sample density (assumed to be 2.7 g/cm^3, representative of the quartzite and gneiss we sampled), sample thickness (ranged from 1.5 to 6.0 cm; Table 2), and topographic shielding caused by the dip of the sample surface (up to 30°; Table 2; with correction factors calculated in the CRONUS Earth online calculator). We made no corrections for snow or till cover because the ridges we sampled were likely windswept and bare. We also made no correction for shielding by surrounding topography, which was negligible.

When comparing exposure ages within the data set, we cite the internal age uncertainties because the samples come from the same area and therefore any errors in production rate scaling will affect all samples similarly. When comparing our age data to other data sets, we cite the external uncertainties (calculated by the CRONUS Earth online exposure age calculator; Balco et al. 2008) that take into account AMS precision as well as additional uncertainty introduced through the chosen production rate and altitude/latitude scaling scheme.

RESULTS

For the samples assessed here (Fig. 2; only those analyzed in 2000, including two replicates), background-corrected 07KNSTD-scaled ^{10}Be concentrations range from 1.06×10^5 to 1.53×10^5 atoms/g, yielding exposure ages of 21.2 to 28.6 ka (n = 18; Table 4, Fig. 3). Background-corrected ^{26}Al concentrations in samples range from 5.61×10^5 to 9.66×10^5 atoms/g, with exposure ages of 16.7 to 29.2 ka (n = 18; Table 4, Fig. 3). The ^{26}Al age range narrows to 20.1 to 29.2 ka if one outlier is omitted, as described in the following paragraph. Exposure ages from the two isotopes are related (Fig. 4); a 1σ York regression yields a slope indistinguishable from 1 (1.12 ± 0.19) and a y-intercept indistinguishable from 0 (-3.9 ± 4.6 ka).

There are two laboratory replicates in the data set. For SMH-9 and SMH-9-DUP, both their ^{10}Be (22.1 ± 0.7 ka and 21.2 ± 0.7 ka) and ^{26}Al (21.2 ± 0.8 ka and 21.9 ± 1.1 ka) exposure ages are indistinguishable within 1σ analytic uncertainties. Because of this close agreement, we use the average exposure age and uncertainty for SMH-9 in our data interpretation (21.6 ± 0.7 ka for ^{10}Be and 21.6 ± 0.9 ka for ^{26}Al). However, for SPA-6 and SPA-6-DUP, a sample with high native ^{27}Al concentration in the quartz, the ^{10}Be (25.2 ± 0.8 ka and 23.1 ± 0.8 ka) and ^{26}Al (16.7 ± 0.7 ka and 20.1 ± 1.5 ka) exposure ages differ at 1σ. The poor agreement in this case, as well as the anomalously young ^{26}Al age of SPA-6 in relation to the rest of the data set (Table 4), suggests that the inferred ^{26}Al concentration of SPA-6 is inaccurate. One possible explanation may be loss of Al in sample SPA-6 (but possibly not the duplicate) during laboratory processing,

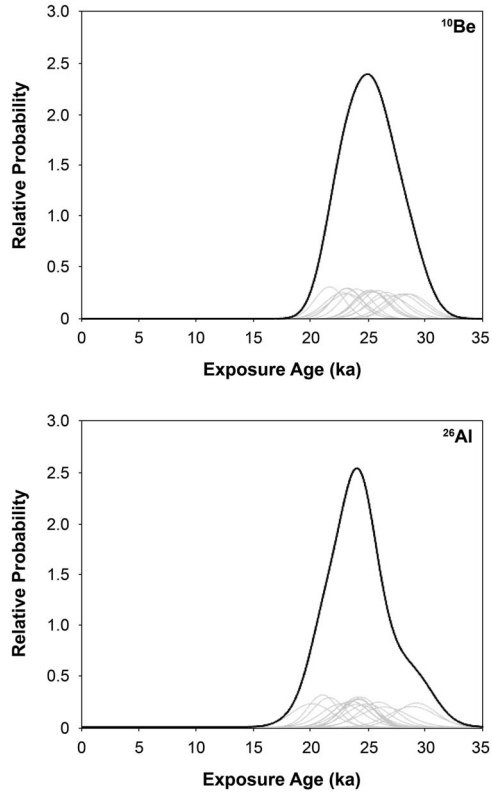

Figure 3. Probability density functions for ^{10}Be (top panel) and ^{26}Al (bottom panel) exposure ages and their external uncertainties. Gray lines denote the 16 samples individually; black line shows the summed probability for the data set as a whole.

perhaps caused by precipitation of fluoride compounds following digestion. Loss of Al in this case is evidenced by the fact that both SPA-6 and SPA-6-DUP had the same mass of quartz, yet the ICP-quantified total Al in SPA-6-DUP is ~40% higher than in SPA-6 (Table 3). We accordingly reject the data for SPA-6 and use only the data for SPA-6-DUP.

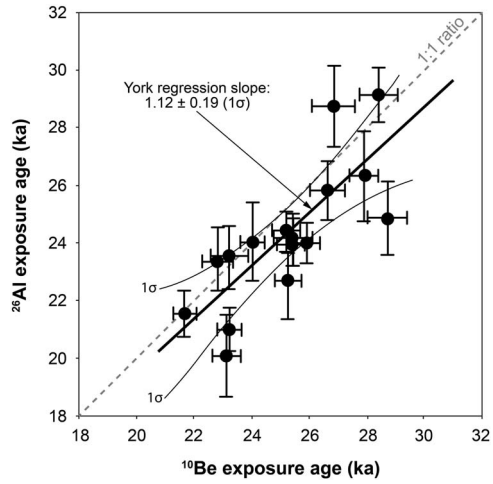

Figure 4. Comparison of ^{10}Be and ^{26}Al exposure ages (n = 16). Gray line shows a 1:1 relationship. Error bars show 1σ internal uncertainties for each isotope. Heavy black line shows a York linear regression, and thin black lines show the 1σ uncertainty envelope around the regression.

In addition to laboratory replicates, we compare the ages of field replicates. Samples SAF-10 and SAF-11 were collected 1 m apart from the top of the same boulder, and their ^{10}Be (25.2 ± 0.7 ka and 25.9 ± 0.7 ka) and ^{26}Al (24.4 ± 0.7 ka and 24.0 ± 0.7 ka) exposure ages are indistinguishable within 1σ analytic uncertainties. Similarly, samples SWR-7 and SWR-8 were collected <1 m apart from the same boulder, and their ^{10}Be (23.2 ± 1.2 ka and 22.8 ± 1.1 ka) and ^{26}Al (23.5 ± 1.1 ka for both) exposure ages are indistinguishable within 1σ analytic uncertainties. The similarity of both the laboratory and the field replicates suggests that age variability within the data set is geologic, not analytic.

Both isotopes yield unimodal age distributions with well-defined peaks (Fig. 3). Considering all 16 samples together, the central tendency of exposure ages is 25.2 ± 2.1 ka (average, 1 SD) for ^{10}Be (8.3% coefficient of variation) and 24.3 ± 2.5 ka for ^{26}Al (10.3% coefficient of variation). These two age populations, determined with the two different isotopes but on the same samples, are indistinguishable from one another when assessed in a two-tailed, independent samples Student's *t*-test (n = 16, $p = 0.26$).

It is important to note that the coefficient of variation for both ^{10}Be and ^{26}Al ages is several times greater than the average analytic precision for both nuclides (for ^{10}Be, 8.3% vs. 2.1%; for ^{26}Al, 10.3% vs. 4.5%). This difference indicates that most of the observed scatter is not analytical but rather must be introduced by geologic processes such as low concentrations of inherited nuclides, differing times of boulder deposition, postglacial erosion of sampled surfaces, or partial shielding by snow and/or till cover (Heyman et al., 2011; Applegate et al., 2012; Briner et al., 2016). Considering only ^{10}Be measurements, the coefficient of variation for the New Jersey terminal moraine dated here (8.3%) is similar to that of the terminal moraine on Martha's Vineyard (8.0%; Balco et al., 2002). Recessional moraines dated cosmogenically (Basin Ponds, Pineo Ridge, Androscoggin, Littleton-Bethlehem, Buzzards Bay, Ledyard, Old Saybrook; n = 7; Fig. 5) have lower coefficients of variation (4.1 ± 2.0, 1 SD).

When both isotopes are considered together, 07KNSTD-scaled ^{26}Al/^{10}Be ratios are 5.9 to 7.3 (when SPA-06 is omitted and only its laboratory replicate is used; Table 4). Based on 1σ analytic uncertainties, 9 of the 16 samples have ^{26}Al/^{10}Be ratios that are indistinguishable from an assumed ^{26}Al/^{10}Be production ratio of 6.75; 1 additional sample (SAF-12) has a ^{26}Al/^{10}Be ratio that exceeds 6.75 beyond 1σ uncertainties. The remaining 6 samples (SPA-3, -4, -5, -6-DUP, and -15, plus SAF-11) have ^{26}Al/^{10}Be ratios that fall below an assumed production ratio of 6.75 beyond 1σ uncertainties.

The ^{10}Be concentrations we present here (samples prepared and analyzed in 2000, scaled to 07KNSTD) are similar to ^{10}Be concentrations from the samples prepared and analyzed in 1995 (scaled to 07KNSTD; detailed in Supplementary Table 1). The two data sets form a linear regression ($R^2 = 0.48$) that is statistically significant

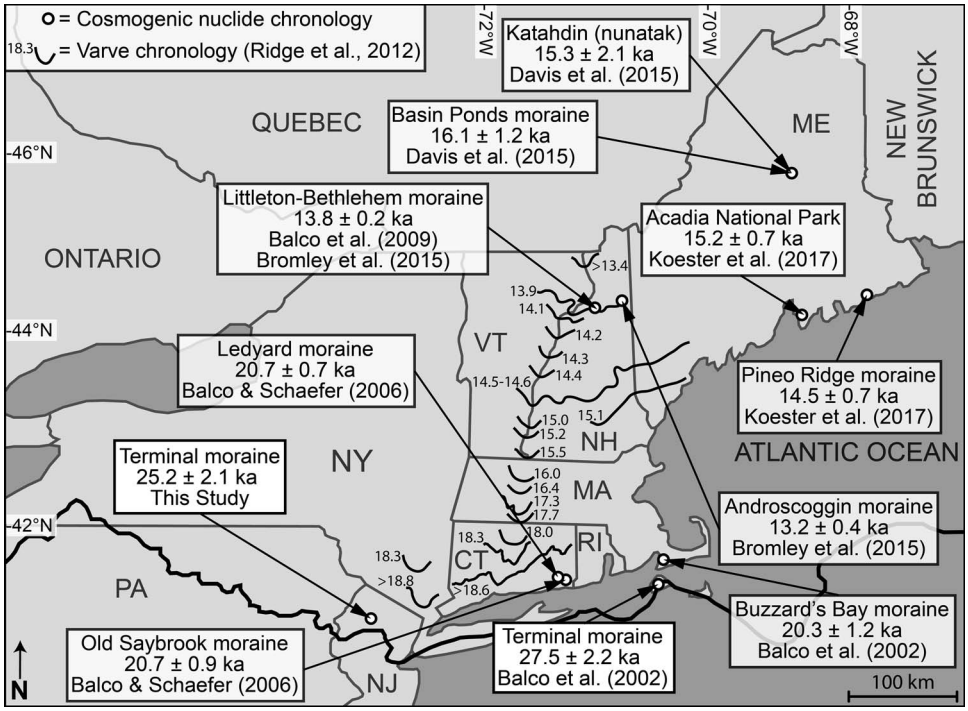

Figure 5. Compilation of cosmogenic ^{10}Be age control for features associated with the maximum extent and subsequent retreat of the Laurentide Ice Sheet in the northeastern United States. Ages show average ± 1 standard deviation, all calculated with the northeastern North American nuclide production rates of Balco et al. (2009); see text for more detail. Also included are ice margin positions based on the North American varve chronology of Ridge et al. (2012). Heavy dark line shows the Laurentide Ice Sheet maximum extent.

($p = 0.01$, n = 13; Supplementary Fig. 3), although three samples (SPA-15, SPA-16, and SWR-7) are not included in this comparison because the 1995 analyses did not yield usable ^{10}Be/^{9}Be data. The average ^{10}Be concentration of the 1995 analyses is $1.24 \pm 0.13 \times 10^5$ atoms/g (n = 13, 1 SD), and the average of the 2000 analyses is $1.22 \pm 0.10 \times 10^5$ atoms/g (n = 13, 1 SD), yielding good agreement despite the intervening five years and numerous methodological developments over that time. The agreement between the ^{26}Al data sets is poorer, yielding no significant linear regression ($R^2 = 0.05$, $P = 0.40$, n = 15 excluding sample SWR-7; Supplementary Fig. 3). The average ^{26}Al concentration of the 1995 analyses is $7.97 \pm 1.31 \times 10^5$ atoms/g (n = 15, 1 SD), and the average of the 2000 analyses is $8.09 \pm 0.87 \times 10^5$ atoms/g (n = 15, 1 SD), yielding two populations that have similar central tendencies but large variance.

DISCUSSION

Assessing cosmogenic nuclide exposure age robustness and limitations

Although numerous geologic factors can affect cosmogenic surface exposure ages (Heyman et al., 2011, 2016; Applegate et al., 2012), we sought to minimize complications with our sampling strategy. Preserved glacial polish and striations on the quartzite bedrock surfaces indicate that postdepositional erosion has not significantly affected these surfaces. Postdepositional movement of boulders also is unlikely because we targeted boulders on topographically high, flat, bedrock ridgetops. We recognized no evidence for extensive erosion of till cover from our sample sites; till is present only in scattered thin patches on the outcrops, and we found no colluvium attributable to the removal of till, nor did we find extensive boulder or gravel lag deposits on outcrops as might be expected if a till matrix had been eroded. All boulders sampled were 1.5–2 m high, making the possibility of postglacial burial by sediment and/or snow, as well as the likelihood of postdepositional movement, small. However, the presence of thick, persistent snow cover in postglacial times cannot be discounted; such snow cover would make our ages too young (Schildgen et al., 2005).

In general, the boulder and bedrock surfaces we sampled were likely free of significant inherited nuclides produced by neutron spallation during previous periods of exposure. The widespread occurence of striations in the study area (Fig. 2; Stone et al., 2002) indicates that the Laurentide Ice Sheet was warm based and erosive, removing weathered and fresh material from most rock surfaces; the range in striation directions (Fig. 2) suggests warm-based ice dominated during advance, stasis, and retreat. Further, the data set does not display patterns typically seen in areas of cold-based, nonerosive ice as reviewed in Corbett et al. (2016a). The population (n = 10) of bedrock ^{10}Be ages is indistinguishable from the population (n = 6) of boulder ^{10}Be ages ($p = 0.17$ using a two-tailed, independent samples Student's *t*-test), suggesting that boulders and bedrock share a common exposure history. Both the ^{10}Be and ^{26}Al data form unimodal

age distributions (Fig. 3) rather than multimodal age distributions indicative of boulder recycling (Marsella et al., 2000; Briner et al., 2005; Corbett et al., 2016a, 2016c). However, the presence of low concentrations of nuclides inherited from deep, muon-induced production during previous interglacials cannot be discounted (Briner et al., 2016), as explored below in more detail.

$^{26}Al/^{10}Be$ ratios are indistinguishable from or slightly exceed an assumed production ratio of 6.75 for 10 of the 16 samples but fall below the production ratio beyond 1σ uncertainties for 6 samples. It is possible the samples with ratios <6.75 experienced burial following initial exposure, thus yielding low ratios because ^{26}Al decays more quickly than ^{10}Be. However, because long burial durations (several hundred thousand years; see fig. 9 in Bierman et al., 1999) are required for burial to be detectable with the $^{26}Al/^{10}Be$ system, we believe that it is unlikely these samples record extended burial. Such long burial durations seem implausible so close to the Laurentide Ice Sheet margin, where the duration of ice cover is limited to the time of maximum glacial conditions.

Rather, we hypothesize that the slightly lower than expected $^{26}Al/^{10}Be$ ratios in our data set may be driven by limitations in the preparation and analysis of the Al samples in the early days of ^{26}Al studies, particularly loss of ^{27}Al through precipitation of fluorides (Bierman and Caffee, 2002). Possible loss of ^{27}Al, especially in samples where the purified quartz contained high native ^{27}Al concentrations, is evidenced by the disagreement between ICP-quantified total ^{27}Al in sample SPA-06 and its duplicate as previously discussed (Table 3), as well as the significant inverse relationship between total ^{27}Al and $^{26}Al/^{10}Be$ ($n = 18$, $R^2 = 0.25$, $p = 0.04$). Poor quantification of total ^{27}Al may be further evidenced by the weak agreement between the inferred ^{26}Al exposure ages from the 1995 and 2000 AMS analyses (Supplementary Fig. 3), although it is impossible to separate laboratory and measurement error. Because of the potential underestimate of total ^{27}Al, we rely on the ^{10}Be data for estimating the age of the terminal moraine; however, the difference between the ^{26}Al and ^{10}Be age estimates is slight (<1 ka, and, as populations of ages, the central tendencies are indistinguishable [$p = 0.26$]).

Cosmogenic nuclide exposure ages and regional relationships

Using an average age for all samples (because the ages form a unimodal population; Fig. 3), we estimate that abandonment of the Budd Lake segment of the terminal moraine occurred before 25.2 ± 2.1 ka (^{10}Be, n = 16, average, 1 SD). This age represents a minimum limiting age for ice recession from the maximum ice extent because our sampled surfaces are slightly north of the terminal moraine (Fig. 2). Although detailed field mapping (Stone et al., 2002; as summarized in Supplementary Fig. 1) indicates the presence of numerous recessional sedimentary units within the study area, these stratigraphic units are not separable by age based on the cosmogenic data we present here because ice retreat occurred more rapidly than the effective resolution of the cosmogenic chronometer.

The age constraints we propose for the terminal moraine in New Jersey are broadly consistent with other ^{10}Be chronologies of Laurentide Ice Sheet maximum extent and retreat in northeastern North America (Fig. 5). Exposure dating with ^{10}Be on the Martha's Vineyard terminal moraine (ages originally from Balco et al. [2002]; recalculated here using the locally calibrated northeastern North American production rates of Balco et al. [2009]) yields an age estimate of 27.5 ± 2.2 ka (eight boulders in the central population, average, 1 SD). This age is indistinguishable from the minimum limit we propose for ice recession from the terminal moraine in north-central New Jersey.

Although other cosmogenic nuclide exposure age studies are not along the same flow line as our study site, ^{10}Be ages (recalculated here as described previously) provide a general picture of ice margin retreat following abandonment of the terminal moraine (Fig. 5). Recessional moraines on Cape Cod, to the east of our study site, yield ages of ~20 ka (Balco et al., 2002). Recessional moraines in southern Connecticut are also ~20 ka (Balco and Schaefer, 2006). The ice margin to the east had reached coastal Maine by ~15–14 ka, exposing the area of Acadia National Park and forming the Pineo Ridge moraine (Koester et al., 2017); ice sheet thinning likely exposed the summit of Katahdin at about the same time (Davis et al., 2015). The Laurentide Ice Sheet margin then reached northern New Hampshire ~13 ka (Balco et al., 2009; Bromley et al., 2015), implying that it took ~12 ka for the Laurentide Ice Sheet margin to retreat across the northeastern United States (Fig. 5).

Reconciling ^{10}Be and ^{14}C chronologies

Reconciling chronological records of glacial history developed with different methods, such as cosmogenic exposure and radiocarbon dating, is challenging because each method has its own assumptions and limitations (Balco and Schaefer, 2006; Peteet et al., 2012). However, in our study area, the agreement between the two approaches is good; the average ^{10}Be age of our sample population, which represents a minimum limit for the age of the terminal moraine (Fig. 2), is compatible with the existing radiocarbon chronology (Table 1, Figs. 1 and 6). The ^{10}Be age of 25.2 ± 2.1 ka (average, n = 16, 1 SD) that we infer is indistinguishable from the maximum limit of 26.02 ± 0.81 cal ka BP from Sirkin and Stuckenrath (1980), the age of 27.07 ± 0.67 cal ka BP from Harmon (1968), and the minimum limit of 24.31 ± 0.63 cal ka BP from Stone et al. (1989). The ^{10}Be age is older than the minimum limits of 22.23 ± 0.22 and 22.43 ± 0.30 cal ka BP from Cotter et al. (1986). However, despite the appearance of good agreement, none of the radiocarbon ages near the study area are from macrofossils; rather, they are amalgamated basal sediment that may have contained ^{14}C-dead material from calcite or recycled organic carbon, making it possible that they are too old. Despite these

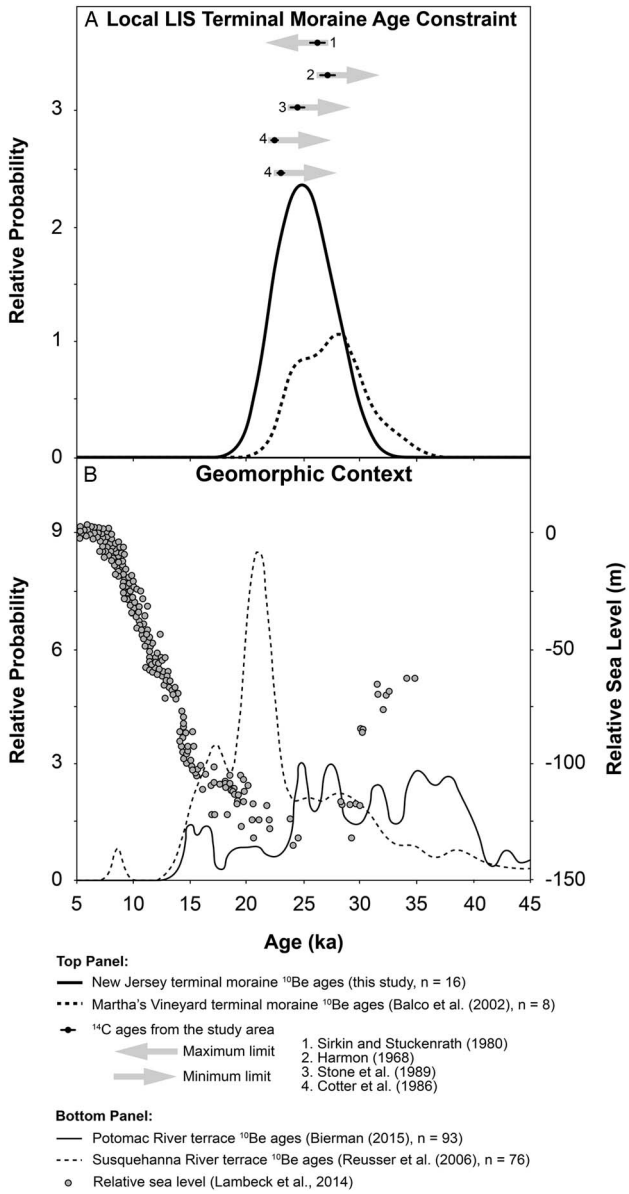

Figure 6. Synthesis of Laurentide Ice Sheet maximum (LIS) extent and geomorphic context. (A) Comparison of constraints on the timing of maximum extent proximal to the study area from different approaches. Cosmogenic nuclide ^{10}Be exposure ages (Table 4) are expressed as summed probability density functions that incorporate each sample's 1σ external uncertainty. Radiocarbon ages (only those local to the study area, Table 1) are shown in calibrated ka BP with error bars that show the 1σ calibrated age range. (B) Regional geomorphic context. Cosmogenic nuclide exposure ages of Potomac and Susquehanna River bedrock strath terraces are expressed as summed probability density functions, rescaled to 07KNSTD as described in the text. Both terrace age distributions have been trimmed to a maximum age of 45 ka.

methodological uncertainties, or perhaps because of them, the ^{10}Be exposure age for the New Jersey terminal moraine supports earlier interpretations of deglaciation timing based on radiocarbon (Sirkin and Stuckenrath, 1980; Cotter et al., 1986; Stone and Borns, 1986; Stone et al., 1989).

Regionally, reconciling cosmogenic nuclide exposure ages and radiocarbon ages is more challenging. Cosmogenic ages of moraines are in coarse agreement with the varve chronology (Fig. 5), although to some extent this is a circular argument because the northeastern North American nuclide production rates of Balco et al. (2009) are partially calibrated against the North American varve chronology (Ridge et al., 2012). The southern Connecticut moraine ages of Balco and Schaefer (2006), 20.7 ± 0.9 and 20.7 ± 0.7 ka (Fig. 5), are consistent with the minimum limit of 18.6 ka from the Connecticut River Valley varves to the north (fig. 12 in Ridge et al., 2012). In northern New Hampshire, the moraine ages of Balco et al. (2009) and Bromley et al. (2015), dating to 13.8 ± 0.2 and 13.2 ± 0.4 ka (Fig. 5), are in agreement with hypothesized ice margin positions in the same region dated to 13.9 and >13.4 ka with varve chronology (fig. 12 in Ridge et al., 2012). Conversely, although less well constrained in the older parts of the record, the reconstructed ice margin positions of Dyke (2004) generally indicate later ice margin retreat than do the cosmogenic ages. Based on a regional compilation of radiocarbon ages (his fig. 4), Dyke (2004) places the ice sheet margin at its maximum extent at 21.4 cal ka BP, which is considerably younger than the age that we infer in New Jersey ($>25.2 \pm 2.1$ ka) and that Balco et al. (2002) infer in Martha's Vineyard (27.5 ± 2.2 ka). Similarly, radiocarbon ages in Dyke (2004) place the ice margin in southern Connecticut at 19.1 cal ka BP, which is 1.6 ka younger than the moraine ages of Balco and Schaefer (2006).

Although many factors likely complicate the agreement between cosmogenic exposure and radiocarbon chronologies, including cosmogenic nuclide production rate uncertainty, one possible explanation is the presence of small but pervasive concentrations of inherited cosmogenic nuclides from previous periods of exposure. Sediment emanating from beneath the Greenland Ice Sheet today has low but detectable concentrations of ^{10}Be, averaging several thousand atoms per gram (Nelson et al., 2014). This is similar to sediment emanating from beneath the Greenland Ice Sheet in the early Holocene (Goehring et al., 2010) and through much of the middle and late Pleistocene (Bierman et al., 2016). Such concentrations are the equivalent of hundreds to as much as a thousand years of surface exposure at sea level. Cobble-sized rocks removed from the modern Greenland Ice Sheet margin appear to have lower but still detectable concentrations of ^{10}Be, averaging several hundred to several thousand atoms per gram (Corbett et al., 2016b). Conversely, boulders recently exposed from beneath a small glacier on southern Baffin Island did not have any detectable ^{10}Be (Davis et al., 1999), although both laboratory blanks and analytic detection limits have lowered considerably since Davis et al. made those measurements.

Low concentrations of inherited ^{10}Be in rock surfaces may be sufficient to explain, at least partially, cosmogenic nuclide exposure ages that exceed radiocarbon ages. If these low concentrations of inherited ^{10}Be were produced by spallation in surface material during past periods of exposure, their presence would indicate low erosion efficiency of glacial ice.

More likely, given abundant evidence of warm-based ice in the field area, any inherited nuclides in our samples were produced by muons, which penetrate deeply into Earth's surface materials (Heisinger et al., 2002). Numerical models of Briner et al. (2016) and Bierman et al. (2016) demonstrate that muon-produced ^{10}Be is likely present in rocks at low but measurable concentrations even after glacial erosion has stripped many meters of surface material, making it possible for inherited ^{10}Be to exist in samples (albeit at very low levels) regardless of glacial erosion efficiency.

The role of muon production in deeply sourced rocks becomes especially important with long interglacial exposure durations (tens of thousands of years), when the low production rate of ^{10}Be from muons (only ~3% of surface spallation rates; Phillips et al., 2016) continues for sufficient time to build up measurable quantities of ^{10}Be (see fig. 4 in Briner et al., 2016). Such long interglacial exposure times typify marginal areas of the former Laurentide, Scandinavian, and Cordilleran Ice Sheets, which ablate completely and reform with each glacial cycle. In contrast, the Greenlandic and Antarctic Ice Sheets remain at least partially intact through most interglacial periods, thereby shielding underlying rock and minimizing nuclide production even by muons. Therefore, muon-produced ^{10}Be likely plays a more significant role in cosmogenic ages of glacial features of mid-latitude ice sheets than of high-latitude ice sheets.

Inherited cosmogenic nuclides produced by muons may make ^{10}Be ages too old by hundreds or perhaps a thousand years (Briner et al., 2016). However, muon-produced ^{10}Be is not sufficient to explain the disagreement between cosmogenic nuclide exposure ages from the Laurentide Ice Sheet terminal moraine of ~25 ka (this study) and ~27 ka (Balco et al., 2002) and radiocarbon ages from the oldest varves of ~19 ka (Ridge et al., 2012). Because the cosmogenic nuclide ages come from the terminal moraine and the oldest varves are tens of kilometers north of the terminal moraine (Fig. 5), it appears that initial ice margin retreat occurred very slowly. Alternatively, the offset could be explained if all samples in this data set as well as those of Balco et al. (2002) contained significant concentrations of inherited ^{10}Be from prior exposure. We consider the latter unlikely given the close agreement between bedrock and boulder ages in our data set and the presence of striations on rock surfaces (Fig. 2).

Climatic and geomorphic context

Both regionally and globally, our results place the abandonment of the Laurentide Ice Sheet terminal moraine in the Highlands of New Jersey during peak glacial conditions. In the Hybla Valley of northern Virginia (Fig. 1), ~320 km southwest of our study site, a 100 ka pollen record based on the abundance of *Quercus* (oak) pollen shows the coldest conditions in the eastern-central United States lasted from ~28 to 21 ka (Litwin et al., 2013). Deglaciation from the terminal moraine occurred in the middle of this interval, before 25.2 ± 2.1 ka (average, n = 16, 1 SD) as determined cosmogenically and within local bracketing radiocarbon ages of ~27–22 cal ka BP (Harmon, 1968; Sirkin and Stuckenrath, 1980; Cotter et al., 1986; Stone et al., 1989).

Climate records from the high northern latitudes indicate generally similar timing of the last glacial maximum to the age we infer for the Laurentide Ice Sheet terminal moraine in New Jersey. Oxygen isotopes from Greenland ice cores suggest that the height of glacial conditions occurred ~22 ka (Camp Century; Dansgaard et al. 1969) or ~26–24 ka (GISP2; Stuiver and Grootes, 2000). Sediments from a compilation of North Atlantic marine cores place the height of glacial conditions ~27–24 ka (Bond et al., 1997), whereas sediments from Lake El'Gygytgyn in Siberia find the height of glacial conditions slightly later, ~22–18 ka (Melles et al., 2007). Compilations of sea-level data define the last glacial maximum as ~26–19 ka (Clark et al., 2009) or ~29–20 ka (Lambeck et al., 2014).

The presence of the Laurentide Ice Sheet in New Jersey and adjacent southeastern Pennsylvania influenced regional geomorphology through the ice sheet's impact on climate, glacial isostacy, and changes in sediment supply. Extensive ^{10}Be dating of strath terraces (Reusser et al., 2006) along the Susquehanna River (Fig. 1), the headwaters of which were partially glaciated, shows that incision started ~25 ka and peaked at ~21 ka (Fig. 6). The timing of Susquehanna River incision is coincident with the local last glacial maximum (according to ages presented here) and with initial ice margin retreat and meltwater generation. This incision may reflect a combination of high, meltwater-augmented flows and/or the presence of glacial sediment that increased erosivity of the floodwaters. South of the glacial limit, the unglaciated Potomac River (Fig. 1) also incised, leaving several strath terrace levels at Great Falls (Bierman, 2015). Incision there mostly predates the glacial maximum with the most significant mode of ^{10}Be exposure ages between 37 and 22 ka (Fig. 6). With the outlet of the Potomac River into Chesapeake Bay located at the zone of maximum glacioisostatic subsidence today (and thus maximum forebulge uplift during glaciation; Engelhart et al., 2009; DeJong et al., 2015), and lacking glacial meltwater influences, incision there must have been controlled by a combination of isostatically driven land surface uplift and the influence of climate on river flow.

Our results suggest that the Laurentide Ice Sheet in the northeastern United States began to retreat from its maximum extent before other large ice sheets. For example, the interconnected Eurasian ice sheets (British-Irish, Svalbard-Barents-Kara Seas, and Scandinavian) did not achieve their maximum extent until ~21 ka (Hughes et al., 2016). The Cordilleran Ice Sheet reached its maximum several thousand years later, ~17–18 ka (Clague and James, 2002). We do not know why the Laurentide Ice Sheet terminal moraines in the northeastern United States are older than other terminal ice sheet moraines, but the pattern may extend to the North Atlantic region as a whole; the western margin of the Eurasian Ice Sheet reached its maximum earlier than the rest of the ice sheet, ~27–26 ka (Hughes et al., 2016) and similar to the age we infer for the southeastern margin of the Laurentide Ice Sheet. The difference in timing may also be

related to ice sheet size (with the Laurentide being the largest of the now-vanished Northern Hemisphere ice sheets), ice flow dynamics, regional differences in climate, and/or differences in the chronological techniques used to constrain the timing of maximum extent.

CONCLUSIONS

Here, we date glacial recession from the Laurentide Ice Sheet terminal moraine in New Jersey. Using ^{10}Be cosmogenic nuclide exposure ages of 16 bedrock and boulder samples, we infer that the Budd Lake segment of the terminal moraine was abandoned before 25.2 ± 2.1 ka (average, 1 SD). This age is in close agreement with bracketing radiocarbon ages from the study region as well as cosmogenic age estimates for the terminal moraine to the east, on Martha's Vineyard. The uncertainty in our age estimate and that of the moraine on Martha's Vineyard is similar (~8%); both are dominated by sample-to-sample age variance rather than analytic precision, most likely caused by the violation of assumptions inherent to exposure dating. The timing of glacial recession from the Laurentide Ice Sheet terminal moraine is consistent with the height of glacial conditions and the resultant sea-level lowstand as documented by other proxy records regionally and globally, and with river incision history in the mid-Atlantic region.

ACKNOWLEDGMENTS

Funding for this work was provided by Geological Society of America Field Research Grant #5394-94 to P. Larsen and National Science Foundation EAR #9396261 to P. Bierman. We thank C. Massey for field assistance and J. Turner for laboratory assistance. Personnel at the Picatinny Arsenal in Dover, New Jersey, provided access to sample sites. Isotopic measurements were made at the Center for Accelerator Mass Spectrometry, Lawrence Livermore National Laboratory with assistance from R. Finkel, J. Koenig, and J. Southon. Previous versions of this manuscript were improved by reviews from B. Atwater, E. Brook, M. Burbach, R. Carswell, K. Marsella, M. Reheis, and J. Stone. We thank J. Briner and one anonymous journal reviewer for constructive comments on the current version, as well as M. Pavich for U.S. Geological Survey review.

SUPPLEMENTARY MATERIALS

For supplementary material/s referred to in this article, please visit https://doi.org/10.1017/qua.2017.11

REFERENCES

Anderson, R., Davis, R., Miller, N., Stuckenrath, R., 1986. History of late- and post-glacial vegetation and disturbance around Upper South Branch Pond, northern Maine. *Canadian Journal of Botany* 64, 1977–1986.

Anderson, R., Jacobson, G., Davis, R., Stuckenrath, R., 1992. Gould Pond, Maine: late-glacial transitions from marine to upland environments. *Boreas* 21, 359–371.

Applegate, P., Urban, N., Keller, K., Lowell, T., Laabs, B., Kelly, M., Alley, R., 2012. Improved moraine age interpretations through explicit matching of geomorphic process models to cosmogenic nuclide measurements from single landforms. *Quaternary Research* 77, 293–304.

Applegate, P., Urban, N., Laabs, B., Keller, K., Alley, R., 2010. Modeling the statistical distributions of cosmogenic exposure dates from moraines. *Geoscientific Model Development* 3, 293–307.

Balco, G., 2011. Contributions and unrealized potential contributions of cosmogenic-nuclide exposure dating to glacier chronology, 1990–2010. *Quaternary Science Reviews* 30, 3–27.

Balco, G., Briner, J., Finkel, R., Rayburn, J., Ridge, J., Schaefer, J., 2009. Regional beryllium-10 production rate calibration for late-glacial northeastern North America. *Quaternary Geochronology* 4, 93–107.

Balco, G., Rovey, C., 2008. An isochron method for cosmogenic-nuclide dating of buried soils and sediments. *American Journal of Science* 308, 1083–1114.

Balco, G., Rovey, C., 2010. Absolute chronology for major Pleistocene advances of the Laurentide Ice Sheet. *Geology* 38, 795–798.

Balco, G., Rovey, C., Stone, J., 2005a. The first glacial maximum in North America. *Science* 307, 222–226.

Balco, G., Schaefer, J., 2006. Cosmogenic-nuclide and varve chronologies for the deglaciation of southern New England. *Quaternary Geochronology* 1, 15–28.

Balco, G., Stone, J., Lifton, N., Dunai, T., 2008. A complete and easily accessible means of calculating surface exposure ages or erosion rates from ^{10}Be and ^{26}Al measurements. *Quaternary Geochronology* 3, 174–195.

Balco, G., Stone, J., Mason, J., 2005b. Numerical ages for Plio-Pleistocene glacial sediment sequences by ^{26}Al/^{10}Be dating of quartz in buried paleosols. *Earth and Planetary Science Letters* 232, 179–191.

Balco, G., Stone, J., Porter, S., Caffee, M., 2002. Cosmogenic-nuclide ages for New England coastal moraines, Martha's Vineyard and Cape Cod, Massachusetts, USA. *Quaternary Science Reviews* 21, 2127–2135.

Bierman, P., 1994. Using in situ produced cosmogenic isotopes to estimate rates of landscape evolution: a review from the geomorphic perspective. *Journal of Geophysical Research* 99, 13885–13896.

Bierman, P., 2015. The incision history of the Great Falls of the Potomac River—the Kirk Bryan field trip. In: Brezinski, D.K., Halka, J.P., Ortt, R.A., Jr. (Eds.), Tripping from the Fall Line: Field Excursions for the GSA Annual Meeting, Baltimore, 2015. Field Guide 40. Geological Society of America, Boulder, CO, pp. 1–10.

Bierman, P., Caffee, M., 2002. Cosmogenic exposure and erosion history of Australian bedrock landforms. *Geological Society of America Bulletin* 114, 787–803.

Bierman, P., Davis, P., Corbett, L., Lifton, N., 2015. Cold-based, Laurentide ice covered New England's highest summits during the Last Glacial Maximum. *Geology* 43, 1059–1062.

Bierman, P., Marsella, K., Patterson, C., Davis, P., Caffee, M., 1999. Mid-Pleistocene cosmogenic minimum-age limits for pre-Wisconsinan glacial surfaces in southwestern Minnesota and southern Baffin Island: a multiple nuclide approach. *Geomorphology* 27, 25–39.

Bierman, P., Shakun, J., Corbett, L., Zimmerman, S., Rood, D., 2016. Marine-sediment ^{10}Be and ^{26}Al records of a persistent and

dynamic East Greenland Ice Sheet since the Pliocene. *Nature* 540, 256–260.

Bond, G., Showers, W., Cheseby, M., Lotti, R., Almasi, P., deMenocal, P., Priore, P., Cullen, H., Hajdas, I., Bonani, G., 1997. A pervasive millennial-scale cycle in North Atlantic Holocene and glacial climates. *Science* 278, 1257–1266.

Briner, J., Bini, A., Anderson, R., 2009. Rapid early Holocene retreat of a Laurentide outlet glacier through an Arctic fjord. *Nature Geoscience* 2, 496–499.

Briner, J., Goehring, B., Mangerud, J., Svendsen, J., 2016. The deep accumulation of ^{10}Be at Utsira, southwestern Norway: implications for cosmogenic nuclide exposure dating in peripheral ice sheet landscapes. *Geophysical Research Letters* 43, 9121–9129.

Briner, J., Gosse, J., Bierman, P., 2006a. Applications of cosmogenic nuclides to Laurentide Ice Sheet history and dynamics. *Geological Society of America Special Papers* 415, 29–41.

Briner, J., Lifton, N., Miller, G., Refsnider, K., Anderson, R., Finkel, R., 2014. Using in situ cosmogenic ^{10}Be, ^{14}C, and ^{26}Al to decipher the history of polythermal ice sheets on Baffin Island, Arctic Canada. *Quaternary Geochronology* 19, 4–13.

Briner, J., Miller, G., Davis, P., Bierman, P., Caffee, M., 2003. Last Glacial Maximum ice sheet dynamics in Arctic Canada inferred from young erratics perched on ancient tors. *Quaternary Science Reviews* 22, 437–444.

Briner, J., Miller, G., Davis, P., Finkel, R., 2005. Cosmogenic exposure dating in arctic glacial landscapes: implications for the glacial history of northeastern Baffin Island, Arctic Canada. *Canadian Journal of Earth Sciences* 42, 67–84.

Briner, J., Miller, G., Davis, P., Finkel, R., 2006b. Cosmogenic radionuclides from fjord landscapes support differential erosion by overriding ice sheets. *Geological Society of America Bulletin* 118, 406–420.

Bromley, G., Hall, B., Thompson, W., Kaplan, M., Hgarcia, J., Schaefer, J., 2015. Late glacial fluctuations of the Laurentide Ice Sheet in the White Mountains of Maine and New Hampshire. *U.S.A. Quaternary Research* 83, 522–530.

Carlson, A., Clark, P., Raisbeck, G., Brook, E., 2007. Rapid Holocene deglaciation of the Labrador sector of the Laurentide Ice Sheet. *Journal of Climate* 20, 5126–5133.

Clague, J., James, T., 2002. History and isostatic effects of the last ice sheet in southern British Columbia. *Quaternary Science Reviews* 21, 71–87.

Clark, D., Bierman, P., Larsen, P., 1995. Improving in situ cosmogenic chronometers. *Quaternary Research* 44, 367–377.

Clark, P., Brook, E., Raisbeck, G., Yiou, F., Clark, J., 2003. Cosmogenic ^{10}Be ages of the Saglek Moraines, Torngat Mountains, Labrador. *Geology* 31, 617–620.

Clark, P., Dyke, A., Shakun, J., Carlson, A., Clark, J., Wohlfarth, B., Mitrovica, J., Hostetler, S., McCabe, A., 2009. The Last Glacial Maximum. *Science* 325, 710–714.

Clark, P., Mix, A., 2002. Ice sheets and sea level of the Last Glacial Maximum. *Quaternary Science Reviews* 21, 1–7.

Colgan, P., Bierman, P., Mickelson, D., Caffee, M., 2002. Variation in glacial erosion near the southern margin of the Laurentide Ice Sheet, south-central Wisconsin, USA: implications for cosmogenic dating of glacial terrains. *Geological Society of America Bulletin* 114, 1581–1591.

Connally, G.G., Sirkin, L.A., 1973. Wisconsinan history of the Hudson-Champlain Lobe. *Geological Society of America Memoir* 136, 47–69.

Corbett, L., Bierman, P., Davis, P., 2016a. Glacial history and landscape evolution of southern Cumberland Peninsula, Baffin Island, Canada, constrained by cosmogenic ^{10}Be and ^{26}Al. *Geological Society of America Bulletin* 128, 1173–1192.

Corbett, L., Bierman, P., Neumann, T., Graly, J., 2016b. Stories under the ice: investigating glacial history and process with cosmogenic nuclides in icebound cobbles. *Geological Society of America Abstracts with Programs*, 48.

Corbett, L., Bierman, P., Rood, D., 2016c. Constraining multi-stage exposure-burial scenarios for boulders preserved beneath cold-based glacial ice in Thule, northwest Greenland. *Earth and Planetary Science Letters* 440, 147–157.

Cotter, J., Ridge, J., Evenson, E., Sevon, W., Sirkin, L., Stuckenrath, R., 1986. The Wisconsinan history of the Great Valley, Pennsylvania and New Jersey, and the age of the "Terminal Moraine." *Bulletin of the New York State Museum* 455, 22–49.

Dansgaard, W., Johnsen, S.J., Moller, J., Langway, C., 1969. One thousand centuries of climate record from Camp Century on the Greenland Ice Sheet. *Science* 166, 377–381.

Davis, P., Bierman, P., Corbett, L., Finkel, R., 2015. Cosmogenic exposure age evidence for rapid Laurentide deglaciation of the Katahdin area, west-central Maine, USA, 16 to 15 ka. *Quaternary Science Reviews* 116, 95–105.

Davis, P.T., Bierman, P.R., Marsella, K.A., Caffee, M.W., Southon, J.R., 1999. Cosmogenic analysis of glacial terrains in the eastern Canadian Arctic: a test for inherited nuclides and the effectiveness of glacial erosion. *Annals of Glaciology* 28, 181–188.

Davis, P.T., Davis, R.B., 1980. Interpretation of minimum-limiting radiocarbon ages for deglaciation of Mt. Katahdin area. *Maine. Geology* 8, 396–400.

DeJong, B., Bierman, P., Newell, W., Rittenour, T., Mahan, S., Balco, G., Rood, D., 2015. Pleistocene relative sea levels in the Chesapeake Bay region and their implications for the next century. *GSA Today* 25, 4–10.

Dorion, C.C., 1997. An Updated High Resolution Chronology of Deglaciation and Accompanying Marine Transgression in Maine. Master's thesis, University of Maine, Orono.

Drake, A., Volkert, R., Monteverde, D., Herman, G., Houghton, H., Parker, R., Dalton, R., 1996. *Bedrock Geologic Map of Northern New Jersey. Miscellaneous Geologic Investigations Map I-2540-A*. US Geological Survey, Reston, VA.

Dyke, A., 2004. An outline of North American deglaciation with emphasis on central and northern Canada. *Quaternary Glaciations: Extent and Chronology* 2, 373–424.

Engelhart, S., Horton, B., Douglas, B., Peltier, W., Törnqvist, T., 2009. Spatial variability of late Holocene and 20th century sea-level rise along the Atlantic coast of the United States. *Geology* 37, 1115–1118.

Evenson, E., Cotter, J., Ridge, J., Sevon, W., Sirkin, L., Stuckenrath, R., 1983. The mode and chronology of deglaciation of the Great Valley, northwestern New Jersey. *Geological Society of America Abstracts with Programs* 15, 133.

Fabel, D., Harbor, J., 1999. The use of in-situ produced cosmogenic radionuclides in glaciology and glacial geomorphology. *Annals of Glaciology* 28, 103–110.

Fullerton, D., 1986. Stratigraphy and correlation of glacial deposits from Indiana to New York and New Jersey. *Quaternary Science Reviews* 5, 23–37.

Goehring, B., Kelly, M., Schaefer, J., Finkel, R., Lowell, T., 2010. Dating of raised marine and lacustrine deposits in east Greenland using beryllium-10 depth profiles and implications for estimates of subglacial erosion. *Journal of Quaternary Science* 25, 865–874.

Gosse, J., Evenson, E., Klein, J., Lawn, B., Middleton, R., 1995a. Precise cosmogenic ^{10}Be measurements in western North

America: support for a global Younger Dryas cooling event. *Geology* 23, 877–880.

Gosse, J., Grant, D., Klein, J., Klassen, R., Evenson, E., Lawn, B., Middleton, R., 1993. Significance of altitudinal weathering zones in Atlantic Canada, inferred from in situ produced cosmogenic radionuclides. *Geological Society of America Abstracts with Programs* 25, A394.

Gosse, J., Grant, D., Klein, J., Lawn, B., 1995b. Cosmogenic ^{10}Be and ^{26}Al constraints on weathering zone genesis, ice cap basal conditions, and Long Range Mountain (Newfoundland) glacial history. Programme, Abstracts, Field Guides, CANQUA CGRG Joint Meeting, St. John's Canada, CA19.

Gosse, J., Phillips, F., 2001. Terrestrial in situ cosmogenic nuclides: theory and application. *Quaternary Science Reviews* 20, 1475–1560.

Grimm, E., Maher, L., Nelson, D., 2009. The magnitude of error in conventional bulk-sediment radiocarbon ages from central North America. *Quaternary Research* 72, 301–308.

Harmon, K., 1968. Late Pleistocene Forest Succession in Northern New Jersey. PhD dissertation. Rutgers University, New Brunswick, NJ.

Heisinger, B., Lal, D., Jull, A., Kubik, P., Ivy-Ochs, S., Neumaier, S., Knie, K., Lazarev, V., Nolte, E., 2002. Production of selected cosmogenic radionuclides by muons: 1. Fast muons. *Earth and Planetary Science Letters* 200, 345–355.

Heyman, J., Applegate, P., Blomdin, R., Gribenski, N., Harbor, J., Stroeven, A., 2016. Boulder height – exposure age relationships from a global glacial ^{10}Be compilation. *Quaternary Geochronology* 34, 1–11.

Heyman, J., Stroeven, A., Harbor, J., Caffee, M., 2011. Too young or too old: evaluating cosmogenic exposure dating based on an analysis of compiled boulder exposure ages. *Earth and Planetary Science Letters* 302, 71–80.

Hughes, A.L.C., Gyllencreutz, R., Lohne, Ø.S., Mangerud, J., Svendsen, J.I., 2016. The last Eurasian ice sheets – a chronological database and time-slice reconstruction, DATED-1. *Boreas* 45, 1–45.

Kaplan, M., Miller, G., 2003. Early Holocene delevelling and deglaciation of the Cumberland Sound region, Baffin Island, Arctic Canada. *Geological Society of America Bulletin* 115, 445–462.

Kaplan, M., Miller, G., Steig, E., 2001. Low-gradient outlet glaciers (ice streams?) drained the Laurentide ice sheet. *Geology* 29, 343–346.

Koester, A., Shakun, J.D., Bierman, P.R., Davis, P.T., Corbett, L.B., Braun, D., Zimmerman, S.R., 2017. Rapid thinning of the Laurentide Ice Sheet in coastal Maine, USA, during late Heinrich Stadial 1. Quaternary Science Reviews, DOI 10.1016/j.quascirev.2017.03.005.

Kohl, C., Nishiizumi, K., 1992. Chemical isolation of quartz for measurement of in-situ-produced cosmogenic nuclides. *Geochimica et Cosmochimica Acta* 56, 3583–3587.

Lal, D., 1988. In situ-produced cosmogenic isotopes in terrestrial rocks. *Annual Review of Earth and Planetary Sciences* 16, 355–388.

Lal, D., 1991. Cosmic ray labeling of erosion surfaces: in situ nuclide production rates and erosion models. *Earth and Planetary Science Letters* 104, 424–439.

Lambeck, K., Rouby, H., Purcell, A., Sun, Y., Sambridge, M., 2014. Sea level and global ice volumes from the Last Glacial Maximum to the Holocene. *Proceedings of the National Academy of Sciences of the United States of America* 111, 15296–15303.

Larsen, P., 1996. In-Situ Production Rates of Cosmogenic ^{10}Be and ^{26}Al over the Past 21,500 Years Determined from the Terminal Moraine of the Laurentide Ice Sheet, North-Central New Jersey, Geology. Master's thesis, University of Vermont, Burlington.

Litwin, R., Smoot, J., Pavich, M., Markewich, H., Brook, G., Durika, N., 2013. 100,000-year-long terrestrial record of millennial-scale linkage between eastern North American mid-latitude paleovegetation shifts and Greenland ice-core oxygen isotope trends. *Quaternary Research* 80, 291–315.

Long, A., 2009. Back to the future: Greenland's contribution to sea-level change. *GSA Today* 19, 4–10.

Margreth, A., Gosse, J., Dyke, A., 2016. Quantification of subaerial and episodic subglacial erosion rates on high latitude upland plateaus: Cumberland Peninsula, Baffin Island, Arctic Canada. *Quaternary Science Reviews* 133, 108–129.

Marquette, G., Gray, J., Gosse, J., Courchesne, F., Stockli, L., Macpherson, G., Finkel, R., 2004. Felsenmeer persistence under non-erosive ice in the Torngat and Kaumajet mountains, Quebec and Labrador, as determined by soil weathering and cosmogenic nuclide exposure dating. *Canadian Journal of Earth Sciences* 41, 19–38.

Marsella, K., Bierman, P., Davis, P., Caffee, M., 2000. Cosmogenic ^{10}Be and ^{26}Al ages for the last glacial maximum, eastern Baffin Island, Arctic Canada. *Geological Society of America Bulletin* 112, 1296–1312.

Melles, M., Brigham-Grette, J., Glushkova, O., Minyuk, P., Nowaczyk, N., Hubberten, H., 2007. Sedimentary geochemistry of core PG1351 from Lake El'gygytgyn—a sensitive record of climate variability in the East Siberian Arctic during the past three glacial–interglacial cycles. *Journal of Paleolimnology* 37, 89–104.

Miller, G., Briner, J., Lifton, N., Finkel, R., 2006. Limited ice-sheet erosion and complex exposure histories derived from in situ cosmogenic ^{10}Be, ^{26}Al, and ^{14}C on Baffin Island, Arctic Canada. *Quaternary Geochronology* 1, 74–85.

Nelson, A., Bierman, P., Shakun, J., Rood, D., 2014. Using in situ cosmogenic ^{10}Be to identify the source of sediment leaving Greenland. *Earth Surface Processes and Landforms* 39, 1087–1100.

Nishiizumi, K., Imamura, M., Caffee, M., Southon, J., Finkel, R., McAninch, J., 2007. Absolute calibration of ^{10}Be AMS standards. *Nuclear Instruments and Methods in Physics Research Section B: Beam Interactions with Materials and Atoms* 258, 403–413.

Nishiizumi, K., Kohl, C., Arnold, J., Dorn, R., Klein, I., Fink, D., Middleton, R., Lal, D., 1993. Role of in situ cosmogenic nuclides ^{10}Be and ^{26}Al in the study of diverse geomorphic processes. *Earth Surface Processes and Landforms* 18, 407–425.

Nishiizumi, K., Winterer, E.L., Kohl, C.P., Klein, J., Middleton, R., Lal, D., Arnold, J.R., 1989. Cosmic ray production rates of ^{10}Be and ^{26}Al in quartz from glacially polished rocks. *Journal of Geophysical Research* 94, 17907–17915.

Parent, M., Lefebvre, R., Rivard, C., Lavoie, M., Guilbault, J., 2015. Mid-Wisconsinan fluvial and marine sediments in the central St-Lawrence lowlands- implications for glacial and deglacial events in the Appalachian uplands. *Geological Society of America Abstracts with Programs* 47, 82.

Peteet, D.M., Beh, M., Orr, C., Kurdyla, D., Nichols, J., Guilderson, T., 2012. Delayed deglaciation or extreme Arctic conditions 21-16 cal. kyr at southeastern Laurentide Ice Sheet margin? Geophysical Research Letters 39, L11706.

Phillips, F., Argento, D., Balco, G., Caffee, M., Clem, J., Dunai, T., Finkel, R., *et al.,* 2016. The CRONUS-Earth project: a synthesis. *Quaternary Geochronology* 31, 119–154.

Phillips, F., Zreda, M., Smith, S., Elmore, D., Kubik, P., Sharma, P., 1990. Cosmogenic chlorine-36 chronology for glacial deposits at Bloody Canyon, eastern Sierra Nevada. *Science* 248, 1529–1532.

Rayburn, J., DeSimone, D., Staley, A., Mahan, S., Stone, B., 2015. Age of an ice dammed lake on the lee side of the Catskill

Mountains, New York, and rough estimates for the rate of ice advance to the last glacial maximum. *Geological Society of America Abstracts with Programs* 47, 713.

Reimer, P., Bard, E., Bayliss, A., Beck, J., Blackwell, P., Ramsey, C., Buck, C., Cheng, H., Edwards, R., Friedrich, M., Grootes, P., Guilderson, T., Haflidason, H., Hajdas, I., Hatte, C., Heaton, T., Hoffman, D., Hogg, A., Hughen, K., Kaiser, K., Kromer, B., Manning, S., Niu, M., Reimer, R., Richards, D., Scott, E., Southon, J., Staff, R., Turney, C., van der Plicht, J., 2013. IntCal13 and Marine13 radiocarbon age calibration curves 0–50,000 years cal BP: Radiocarbon 55, 1869–1887.

Reusser, L., Bierman, P., Pavich, M., Larsen, J., Finkel, R., 2006. An episode of rapid bedrock channel incision during the last glacial cycle, measured with ^{10}Be. *American Journal of Science* 306, 69–102.

Ridge, J., Balco, G., Bayless, R., Beck, C., Carter, L., Cean, J., Voytek, E., Wei, J., 2012. The new North American varve chronology: A precise record of southeastern Laurentide Ice Sheet deglaciation and climate 18.2–12.5 kyr BP, and correlations with Greenland Ice Core records. *American Journal of Science* 312, 685–722.

Salisbury, R.D., 1902. The Glacial Geology of New Jersey. Final Report. New Jersey Geological Survey, Trenton, NJ.

Schildgen, T., Phillips, W., Purves, R., 2005. Simulation of snow shielding corrections for cosmogenic nuclide surface exposure studies. *Geomorphology* 64, 67–85.

Sirkin, L., Stuckenrath, R., 1980. The Port Washingtonian warm interval in the northern Atlantic coastal plain. *Geological Society of America Bulletin* 91, 332–336.

Staiger, J., Gosse, J., Johnson, J., Fastook, J., Gray, J., Stockli, D., Stockli, L., Finkel, R., 2005. Quaternary relief generation by polythermal glacier ice. *Earth Surface Processes and Landforms* 30, 1145–1159.

Stanford, S., 1993. Late Wisconsinan glacial geology of the New Jersey highlands. *Northeastern Geology* 15, 210–223.

Stanford, S., Witte, R., 2006. *Surficial Geology of New Jersey*. New Jersey Department of Environmental Protection/New Jersey Geological Survey, Trenton, NJ.

Steig, E.J., Wolfe, A.P., Miller, G.H., 1998. Wisconsinan refugia and the glacial history of eastern Baffin Island, Arctic Canada: coupled evidence from cosmogenic isotopes and lake sediments. *Geology* 26, 835–838.

Stone, B., Borns, H., 1986. Pleistocene glacial and interglacial stratigraphy of New England, Long Island, and adjacent Georges Bank and Gulf of Maine. *Quaternary Science Reviews* 5, 39–52.

Stone, B., Reimer, G., Pardi, R., 1989. Revised stratigraphy and history of glacial Lake Passaic, New Jersey. *Geological Society of America Abstracts with Programs* 21, 2.

Stone, B., Stanford, S., Witte, R., 1995. Surficial Geologic Map of the Northern Sheet, New Jersey, U.S. U.S. Geological Survey Map OF-95-543-B, scale 1:100,000. U.S. Geological Survey, Reston, VA.

Stone, B., Stanford, S., Witte, R., 2002. Surficial Geologic Map of Northern New Jersey. U.S. Geological Survey Miscellaneous Investigations Map I-2540-C. U.S. Geological Survey, Reston, VA.

Stone, J., 2000. Air pressure and cosmogenic isotope production. *Journal of Geophysical Research* 105, 23753–23759.

Stone, J., Schafer, J., London, E., DiGiacomo-Cohen, M., Thompson, W., 2005. Quaternary Geologic Map of Connecticut and Long Island Sound Basin. U.S. Geological Survey Miscellaneous Investigations Map I-2784. U.S. Geological Survey, Reston, VA.

Stuiver, M., Grootes, P., 2000. GISP2 oxygen isotope ratios. *Quaternary Research* 53, 277–284.

Ullman, D., Carlson, A., Hostetler, S., Clark, P., Cuzzone, J., Milne, G., Winsor, K., Caffee, M., 2016. Final Laurentide ice-sheet deglaciation and Holocene climate-sea level change. *Quaternary Science Reviews* 152, 49–59.

Ullman, D., Carlson, A., LeGrande, A., Anslow, F., Moore, A., Caffee, M., Syverson, K., Licciardi, J., 2015. Southern Laurentide ice-sheet retreat synchronous with rising boreal summer insolation. *Geology* 43, 23–26.